University of BRISTOL

# A Performance Evaluation of OFDM and FBMC systems in the Underwater Acoustic Channel

**Jack Perrin**

**May 2019**

**Final year project thesis submitted in support of the degree of Master of Engineering in Electrical and Electronic Engineering**

**Department of Electrical & Electronic Engineering**
**University of Bristol**

**DECLARATION AND DISCLAIMER**

Unless otherwise acknowledged, the content of this thesis is the original work of the author. None of the work in this thesis has been submitted by the author in support of an application for another degree or qualification at this or any other university or institute of learning.

The views in this document are those of the author and do not in any way represent those of the University.

The author confirms that the printed copy and electronic version of this thesis are identical.

Signed:

Dated:

**ACKNOWLEDGEMENTS**

I would like to express my heartfelt thanks to all those who have supported me during my time at the University of Bristol

I would like to thank my supervisor Dr. Angela Doufexi along with PhD student Mohammud J Bocus for their many suggestions, guidance and continuous support during this research project. I wish Mohammud all the best in the future on completion of his PhD.

Jack Perrin

## ABSTRACT

# TABLE OF CONTENTS

## LIST OF TABLES

## LIST OF FIGURES

## LIST OF ABBREVIATIONS

| | |
|---|---|
| AFB | Analysis Filter Bank |
| ARQ | Automatic Repeat Request |
| AUV | Autonomous Underwater Vehicle |
| AWGN | Additive White Gaussian Noise |
| BER | Bit Error Rate |
| CP | Cyclic Prefix |
| DAB | Digital Audio Broadcast |
| DFE | Decision Feedback Equalisation |
| DFT | Discrete Fourier Transform |
| DSP | Digital Signal Processing |
| DVB-S2 | Digital Video Broadcasting Second Generation |
| DVB-T | Digital Video Broadcasting Terrestrial |
| EM | Electromagnetic |
| FBMC | Filter Bank Multi Carrier |
| FDM | Frequency Division Multiplexing |
| FEC | Forward Error Correction |
| FFT | Fast Fourier Transform |
| FIR | Finite Impulse Response |
| FMT | Filtered Multi Tone |
| FS | Frequency Spreading |
| ICI | Inter-Channel Interference |
| IFFT | Inverse Fast Fourier Transform |
| IOTA | Isotropic Orthogonal Transform Algorithm |
| ISI | Inter-Symbol Interference |
| LDPC | Low Density Parity Check |
| LLR | Log Likelihood Ratio |
| LMS | Least Mean Squares |
| LTE | Long Term Evolution |
| MAP | Maximum A Posteriori |
| MCM | Multicarrier Modulation |
| MIMO | Multiple Input Multiple Output |
| ML | Maximum Likelihood |
| MMSE | Minimum Mean Squared Error |
| OFDM | Orthogonal Frequency Decision Multiplexing |
| OFDM-CP | Orthogonal Frequency Decision Multiplexing- Cyclic Prefix |
| OFDM-OQAM | OFDM-Offset Quadrature Amplitude Modulation |
| PHYDAS | Physical Layer for Dynamic Access and Cognitive Radio |
| PPN | Polyphase Network |
| PPT | Parts Per Thousand |
| PSD | Power Spectral Density |
| PSK | Phase Shift Keying |
| QAM | Quadrature Amplitude Modulation |
| QOS | Quality Of Service |
| ROV | Remotely Operated Vehicle |
| RSC | Recursive Systematic Convolutional |

| | |
|---|---|
| SCM | Single Carrier Modulation |
| SEMAT | Smart Environmental Measurement and Analysis Technologies |
| SFB | Synthesis Filter Bank |
| SNR | Signal To Noise Ratio |
| SOC | System On Chip |
| SOVA | Soft Output Viterbi Algorithm |
| UWA | Underwater Acoustic |
| UWAC | Underwater Acoustic Channel |
| ZF | Zero Forcing |
| ZP | Zero Padding |

# CHAPTER 1

# THESIS INTRODUCTION

With the great scientific and technological advances of the last 50 years a wide range of underwater applications have emerged. These range from deep sea ocean exploration, and the discovery of the Titanic by Robert Ballard in 1985 [2], to the more recent development of smart environmental measurement and analysis technologies (SEMAT) [3]. The number of underwater applications is ever increasing.

The reliance of these applications on high performing underwater wireless communication links cannot be underestimated. If above ground the communication needs of these applications can be easily supported however the underwater channel provides challenges. To start, both electromagnetic and optical waves are very highly attenuated underwater and, although being far from perfect, acoustic waves are the preferred choice. Acoustic waves are attributed to having low propagation speeds while also suffering from significant multipath effects and frequency dependent attenuation. This is far from ideal and results in signals exhibiting very large Doppler and delay spreads relative to the open air radio channel. To make matters worse, the frequency dependent attenuation leads to a very limited available bandwidth.

As of today Orthogonal Frequency Decision Multiplexing (OFDM) is a popular choice for underwater communications due to its robustness against inter-symbol interference (ISI) and its simple frequency domain equalization. OFDM's robustness against ISI can be owed to the addition of a cyclic prefix (CP) however this leads to a decrease in spectral efficiency. To combat this, an alternative to OFDM-CP known as OFDM-Offset Quadrature Amplitude Modulation (OFDM-OQAM) has been proposed. With the addition of a pair of pulse shaping filter-banks at the transmitter and the receiver OFDM-OQAM has been shown to offer a much improved spectral efficiency without a loss in system performance. This is a particularly attractive offering for communications' engineers seeking to provide maximum throughput in bandwidth limited channels such as the UWAC.

## THESIS OVERVIEW

This thesis examines the performance of OFDM-CP and OFDM-OQAM systems in both horizontally and vertically configured underwater acoustic channels. Chapter 1 begins with a discussion as to why acoustic waves are preferred for underwater communications after which the most challenging aspects of the UWAC are examined.

Chapters 2 and 3 offer detailed analyses of the fundamental techniques behind each system. In addition to this, the pivotal role played by each filter-bank in OFDM-OQAM and the benefit of forward error correction (FEC) coding is addressed.

The results attained from simulations of both OFDM-CP and OFDM-OQAM systems in a variety of channels are shown in chapter 4. Final conclusions and possible future work are detailed in chapter 5.

# CHAPTER 2

# THE UNDERWATER ACOUSTIC CHANNEL

In the past, underwater communications have typically been established with cables. An example of this is remotely operated vehicles (ROVs) being tethered to their mothership with cables used for both power and data transmission. Although required, cables are expensive to maintain and deploy [4] while also limiting the stand-off distance (depth) to which the ROV can operate. With the emergence of new technologies, such as autonomous underwater vehicles (AUVs), there is growing demand for wireless underwater communications. This chapter begins with a detailed evaluation of why acoustic waves are the preferred choice for wireless underwater communications. After this we explore the main UWAC characteristics that we must consider when looking to establish a high performing wireless underwater communications link.

## 2.1 UNDERWATER COMMUNICATION MEDIA

Despite electromagnetic (EM) waves having very beneficial characteristics in the open air environment in seawater they exhibit very different characteristics. The same can be said for optical waves which exhibit characteristics ideal for high speed optical broadband but again are not ideal in sea water environments.

The characteristics of each wave type in sea water are shown in Table 1. The dissolved salt ions and other compounds in sea water increase its conductivity compared to fresh water [1]. It is this high conductivity which results in EM waves being highly attenuated in sea water and having an effective range of only a few metres at low frequencies (around 10kHz). Optical waves, operating around 500nm, likewise are highly attenuated and only capable of propagating up to 100m. Although these waves offer a large available bandwidth underwater and, with it, the potential for high data rates, they do suffer too much attenuation compared to acoustic waves. This is the reason acoustic waves are the wave of choice for underwater communications despite having a limited available bandwidth (in the KHz) and low propagation speed.

| | Acoustic | Electromagnetic | Optical |
|---|---|---|---|
| **Nominal Speed m/s** | 1500 | 33 333 333 | 33 333 33 |
| **Power loss** | Small | Large | ∝Turbidity |
| **Bandwidth** | ~KHz | ~MHz | 10-150 MHz |
| **Frequency Band** | ~KHz | ~MHz | ~$10^{14}$-$10^{15}$ MHz |
| **Effective Range** | ~Km | ~10m | ~10-100m |

Table 1- Wave Characteristics in Sea Water [1]

## 2.2 UNDERWATER ACOUSTIC CHANNEL CHARACTERISTICS

The Underwater Acoustic Channel (UWAC) is often regarded as one of the most challenging environments for communications. When compared to more traditional communication via radio channels the UWAC experiences significantly larger Doppler and delay spreads as well as severe frequency dependent attenuation resulting in a very limited available bandwidth. To make matters worse, the relatively low propagation speed of acoustic waves underwater leads to high proportion multipath delays.

### 2.2.1 ATTENUATION

Three factors must be examined when discussing the attenuation associated with the UWAC. These are spreading loss, absorption and scattering. Spreading loss can be attributed to the geometrical spreading of acoustic waves underwater which results in the transfer of acoustic energy to heat [5]. It is said to be 'cylindrical' in shallow water and 'spherical' in deep water and is only distance dependent [6].

The absorption loss in the UWAC is both distance and frequency dependent. It has been shown to equal $e^{a(f)l}$, where $l$ is the transmission distance, f is the frequency and $a(f)$ is the absorption coefficient. A variety of models have been used to derive the absorption coefficient including Thorps Model and the Fisher and Simmons Model. Thorps model is derived in Equation 1, for frequencies above 100Hz and assumes a sea water temperature of 4°C [7].

$$10\log a(f) = 0.11\frac{f^2}{1+f^2} + 44\frac{f^2}{4100+f^2} + 2.75\cdot 10^{-4} f^2 + 0.003$$

Equation 1

Figure 1 shows the absorption coefficient $a(f)$ as a function of frequency $f$. It can be seen that as the frequency of operation increases the absorption coefficient also quickly rises. This limits the available bandwidth for a set transmission distance, since higher frequencies are highly attenuated.

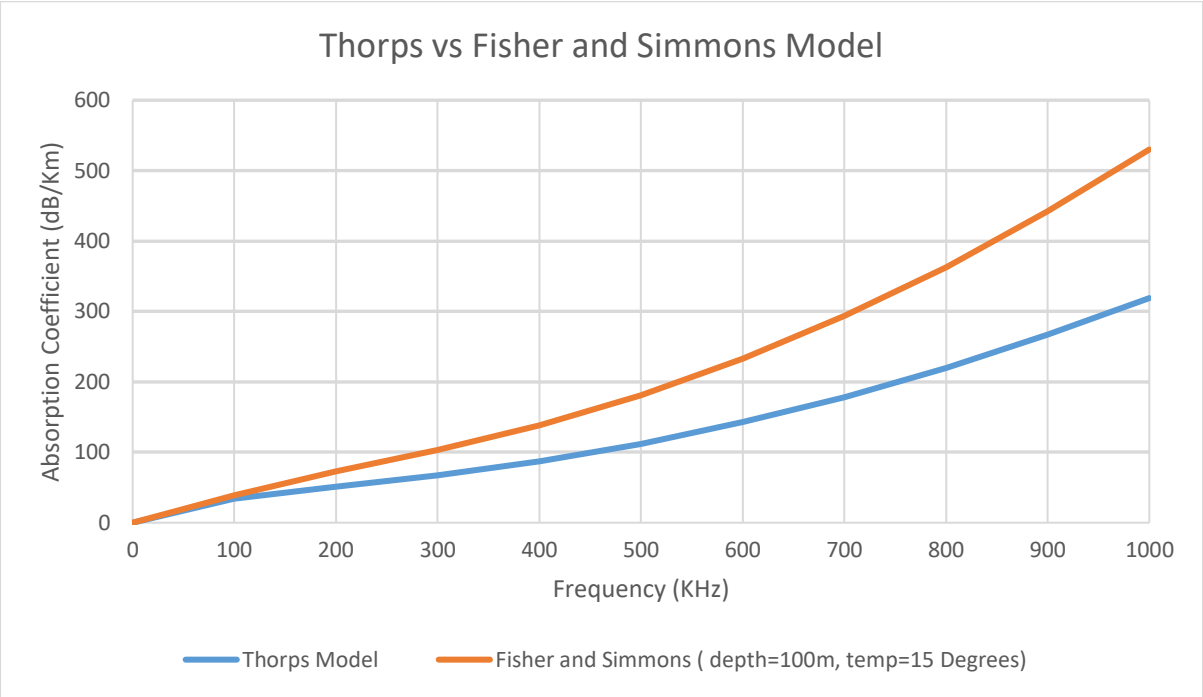


Figure 1- Absorption Coefficient vs Frequency

For frequencies below 50Hz Thorps model can be simplified further:

$$10loga(f) = 0.11\cdot\frac{f^2}{1+f^2} + 0.11f^2 + 0.002$$

Equation 2

In this thesis the Fisher and Simmons model will be used as the model of choice for absorption loss in the UWAC as it takes into account the spatial variation of sound speed in water thus making it more accurate. It is expressed as follows;

$$a(f) = \frac{A_1 P_1 f_1 f^2}{f_1^2 + f^2} + \frac{A_2 P_2 f_2 f^2}{f_2^2 + f^2} + A_3 P_3 f^2$$

Equation 3

where $f_1$ and $f_2$ are the relaxation frequencies of boric acid and magnesium sulphate; $P_1$, $P_2$ and $P_3$ are the pressure depths for boric acid, magnesium sulphate and pure water; $A_1$, $A_2$ and $A_3$ are the components of boric acid, magnesium sulphate and pure water within sea water [7].

The final factor that affects the attenuation of acoustic waves underwater is scattering. Scattering is the process by which acoustic waves are reflected in multiple directions by irregular surfaces. This includes objects such as fish and plankton as well as bubble clouds generated by breaking waves [8]. The amount of scattering is both frequency and object size dependent.

With all these factors in mind, the overall path loss in the UWAC is equal to:

$$10logA(l, f) = k \cdot 10\log(l) + l \cdot 10\log(a(f))$$

Equation 4

where $A(l, f)$ is the path loss in dB as a function of signal frequency $f$, transmission distance $l$, propagation constant $k$ and absorption coefficient $a(f)$ in dB/km. In this case the propagation constant $k$ is also referred as the geometrical spreading factor, and typically has a value of 1.5 [9].

### 2.2.2 NOISE

The UWAC is subject to two different types of noise; ambient noise and site-specific noise [5]. Ambient noise is as a result of multiple sources including waves breaking, turbulence, shipping and thermal noise [1]. It is said to follow a Gaussian distribution, however is ‘not white’ [5] implying it doesn’t have uniform power spectral density (PSD). The ambient noise attributed to each noise source is defined in Equation 5.

$$10logN_t(f) = 17 - 30\log(f)$$

$$10logN_s(f) = 40 + 20(s - 0.5) + 26\log(f) - 60\log(f - 0.03)$$

$$10logN_{wb}(f) = 50 + 7.5w^{0.5} + 20\log(f)$$

$$10logN_{th}(f) = -15 + 20\log(f)$$

Equation 5

where $s$ is the shipping coefficient and takes a value between 0 and 1 depending on the level of shipping activity, $w$ is the wind speed in m/s and $N_t, N_s, N_{wb}$ and $N_{th}$ are the noise levels from each source. NB. The PSD is measured in dB re μ Pa per Hz.

Most acoustic systems typically operate between 100Hz and 100KHz [1]. This region is dominated by noise generated from the breaking of waves with noise from other sources being negligible.

The total ambient noise PSD is defined as follows [8]:

$$N(f) = N_t(f) + N_s(f) + N_{wb}(f) + N_{th}(f)$$

Equation 6

Figure 2 shows the variation in PSD of ambient noise for a variety of wind speeds. It can be seen that noise is much larger at lower frequencies. Since the acoustic waves used in the UWAC typically have a frequency between 100Hz and 100 KHz, this noise limits the achievable throughput.

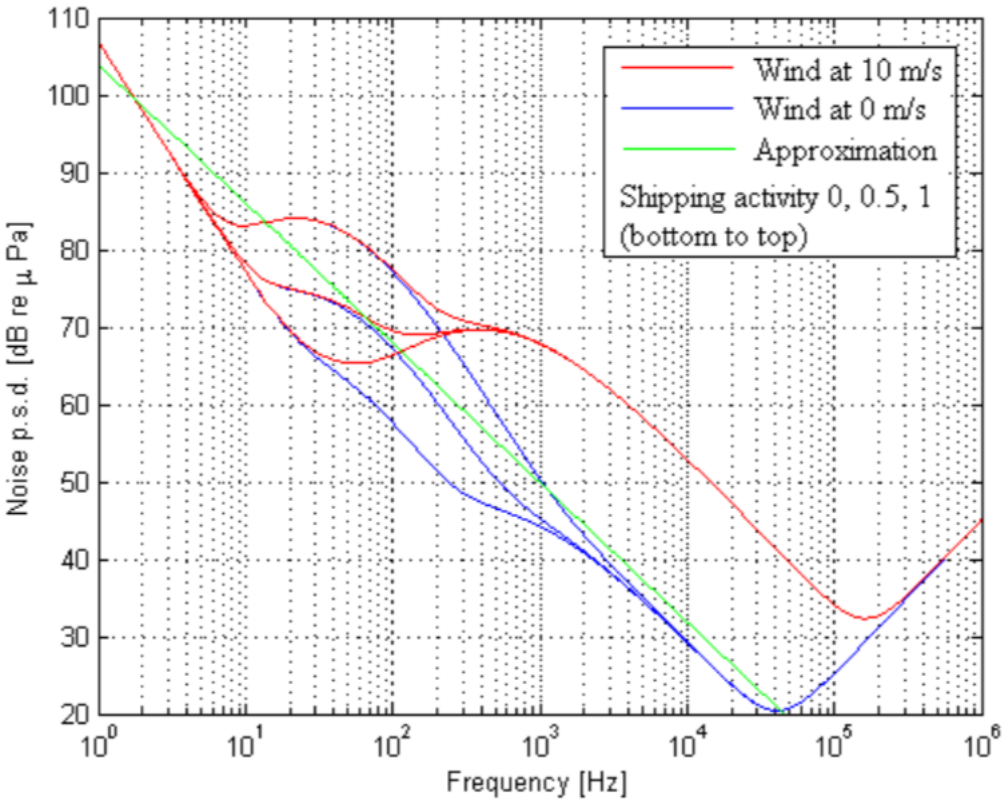


Figure 2- Power Spectral Density of Ambient Noise [SOURCE : *[9]* ]

The second type of noise known as site-specific noise does not follow a Gaussian distribution and is said to cause significant and noticeable interference in the received signal at specific locations only. Examples of this type of noise are snapping shrimp [10] and exterior sonar communications [1], such as those used by the military.

### 2.2.3 DOPPLER SPREAD

The relative motion between transmitter and receiver caused by winds, tides and currents results in a non-negligible Doppler spread in the UWAC [4]. In fact it is known from [11] that the Doppler Spread in the UWAC is significantly greater than that experienced in the open air radio channel. This is as a result of the difference in propagation speeds of acoustic and radio waves; with acoustic waves travelling at ~ 1500m/s in water compared to radio waves at ~ 3x10^8 m/s in air. Referring to Equation 7, the Doppler factor α, for a relative velocity of 0.5m/s, will be around $1.6 \cdot 10^{-9}$ in the open air radio channel however it will be several magnitudes greater at $3 \cdot 10^{-4}$in the UWA channel.

$$\alpha = \frac{v}{c}$$

Equation 7

where $a$ Doppler factor, $v$ is the relative velocity between transmitter and receiver in m/s and $c$ is the speed of sound also in m/s [5].

For a discrete set of multipaths, the Doppler factor is related to the channel response with the following equation:

$$c(\tau, t) = \sum_{p=1}^{N_p} A_p \delta(\tau - [\tau_p - \alpha_p t])$$

Equation 8

where $N_p$ is the number of discrete paths, $A_p$ is each paths amplitude , $\tau_p$ is the path delay and $\alpha_p$ is each single paths Doppler factor.

A received signal with a large Doppler spread will be subject to frequency shifts which, if uncorrected, will cause inter-channel interference (ICI) and thus performance degradation. This is particularly prevalent in multi-carrier acoustic systems, where each subcarrier will experience a different Doppler shift, and with it uncorrelated distortion across the available bandwidth [12]. This is known as frequency spreading and can be limited with the implementation of Doppler compensation algorithms before demodulation .

### 2.2.4 DELAY SPREAD

Multipath propagation is the process 'which results in acoustic signals reaching the receiver by two or more paths (…) each of them with different amplitudes, phases and instants of arrival' [9]. Figure 3 illustrates the two scenarios in which multipath propagation occurs in the UWAC.

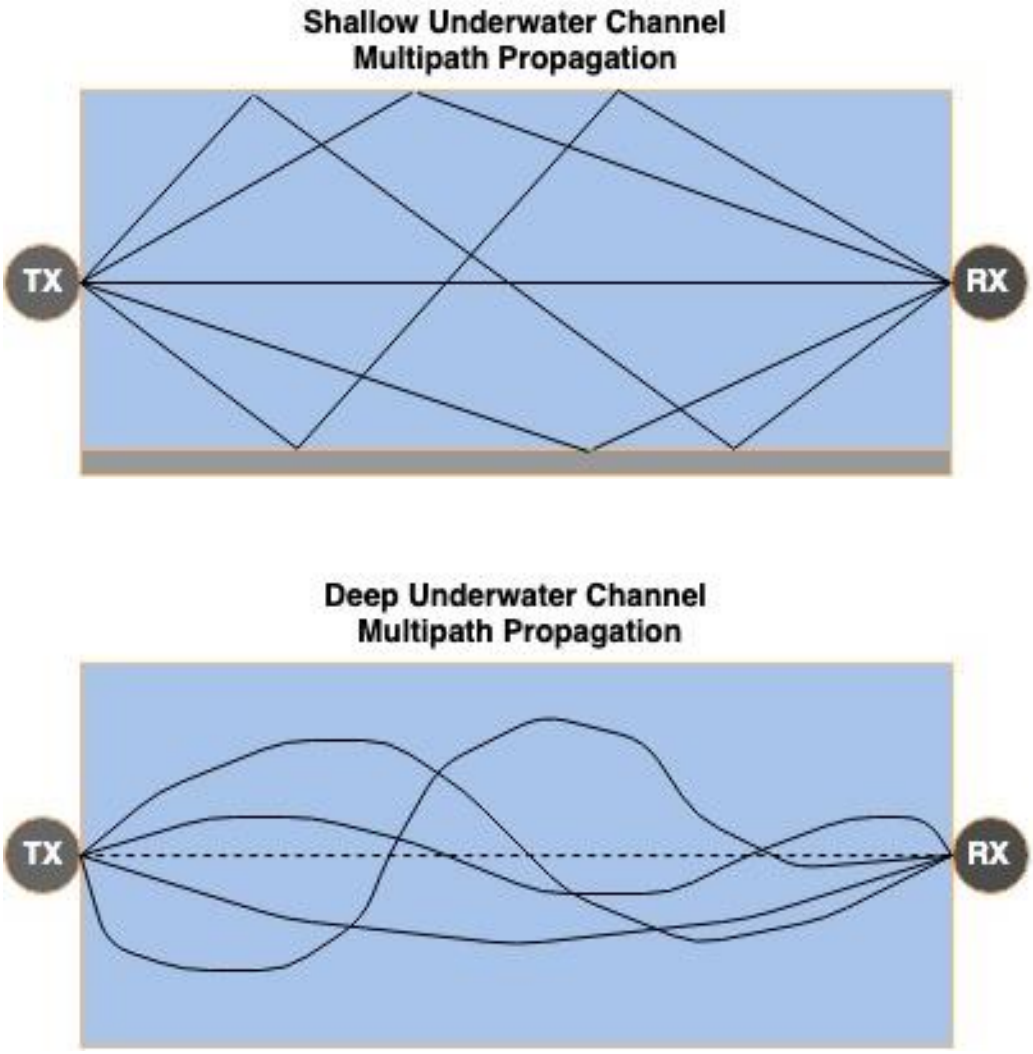


Figure 3- Multipath Propagation in the UWAC

In shallow water, where the depth of water is smaller than the transmission distance [1], waves being reflected off both the ocean surface and ocean floor generate multipaths [9].

In deep water multipaths generated by reflection can be neglected. Figure 4 shows the spatial variation of the speed of acoustic waves underwater. It can be seen that the speed of acoustic waves varies much more at greater ocean depths. This results in multipath propagation occurring as a result of refraction with the acoustic waves bending towards the area of lower propagation speed thus obeying Snell's law [5].

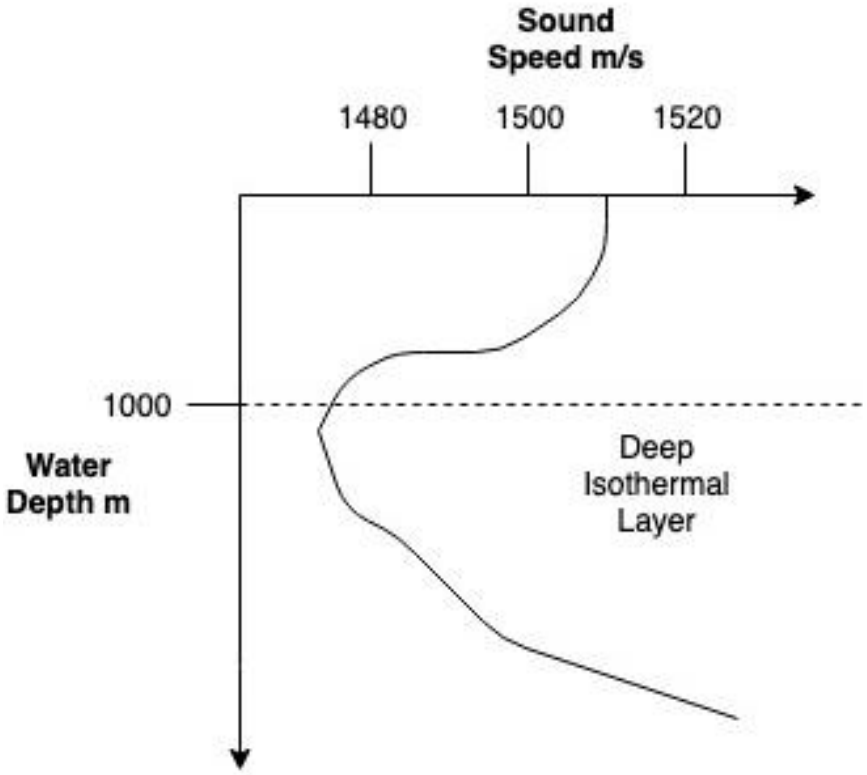


Figure 4- Spatial Variation of Speed of Sound Underwater

Multipath propagation produces a delay spread that is equal to the maximum delay between the arrival times of the paths at the receiver. This is shown in Equation 9.

$$D_s = \max\{[\tau_p - \tau_q]\}$$

Equation 9

where $\tau_p$ and $\tau_q$ are different path delays.

In the open air radio environment channel delay spread is usually several microseconds however in the UWA channel it can reach hundreds of milliseconds. Without the implementation of methods to reduce this time dispersion severe intersymbol interference (ISI) will occur resulting in severe degradation in system performance.

The speed of sound in water can be described using Mackenzie's equation. It shows that the speed of sound is depth, temperature and salinity dependent.

$$v = 1.448.96 + (4.591 \cdot T_c) - \left(5.304 \cdot 10^{-2} \cdot {T_c}^2\right) + \left(2..374 \cdot 10^{-4} \cdot {T_c}^3\right)$$
$$+\left(\left(1.34 \cdot (S - 35)\right) + (1.63 \cdot 10^{-2} \cdot h) + (1.675 \cdot 10^{-7} \cdot h^2)\right.$$
$$-\left((1.025 \cdot 10^{-2} \cdot T_c) \cdot (S - 35)\right) - (7.139 \cdot 10^{-13} \cdot T_c \cdot h)$$

Equation 10

where $v$ is the speed of sound in m/s, $T_c$ is sea water temperature in °C, $h$ is the depth in m and $S$ is the salinity in PPT (parts per thousand).

# CHAPTER 3

# ORTHOGONAL FREQUENCY DIVISION MULTIPLEXING

OFDM is not a new technique. First proposed in 1966 by Chang of Bell Labs (NOKIA), the theory of multiple carriers operating on orthogonal sub bands has been around for a while [13]. It was five years later in 1971 when Chang's theory really gained potential with Weinstein and Ebert successfully testing the use of FFT [13]. The limitations of practical electronics and the large computation requirements for FFT at that time [14], meant OFDM was no good for general use. The first successful tests of OFDM occurred in 1990 in the Eureka-147 projects research into new digital audio broadcast (DAB) radio techniques [15]. Despite this it was only in September of 1995, with the introduction of the BBC's first DAB digital radio broadcast, that OFDM saw its first use in industry. Since then, and with the rise in computing power, OFDM has become one of the most popular multi carrier modulation (MCM) techniques used within communications and is set to be used for generations to come.

This chapter begins with a general description of OFDM as a MCM technique, after which we investigate the fundamental OFDM modulation techniques. This is followed by the analysis of popular forward error correction codes and problems with OFDM in the UWA channel.

## 3.1 GENERAL OVERVIEW

OFDM is based upon the idea of splitting the available bandwidth into many smaller, equally spaced sub-bands, known as subcarriers, which each carry part of the transmitted signal [1]. Compared to traditional single carrier modulation (SCM) techniques, OFDM transmits symbols in parallel on many different subcarriers but at a lower symbol rate. As such, an OFDM system with 256 carriers will have a symbol period around 256 times larger than an SCM system providing an equivalent data rate.

OFDM is a popular MCM technique within the communications industry and is present in Long Term Evolution (LTE), DVB-T and 802.11a Wi-Fi standards [16] [17]. It is particularly

popular due to its robustness against ISI with the addition of a guard interval along with its high bandwidth efficiency and simple frequency domain equalisation.

### 3.2 OFDM FUNDAMENTALS

#### 3.2.1 ORTHOGONALITY

Since OFDM does not employ guard bands, which are used in traditional frequency division multiplexing (FDM) techniques, it is paramount that orthogonality is maintained between subcarriers such that inter channel interference (ICI) is limited [13]. Figure 5 shows the relevant subcarriers in an OFDM system in the frequency domain. Orthogonality can be seen to be maintained since the amplitude of all other subcarriers is 0 at the centre frequency of each subcarrier.

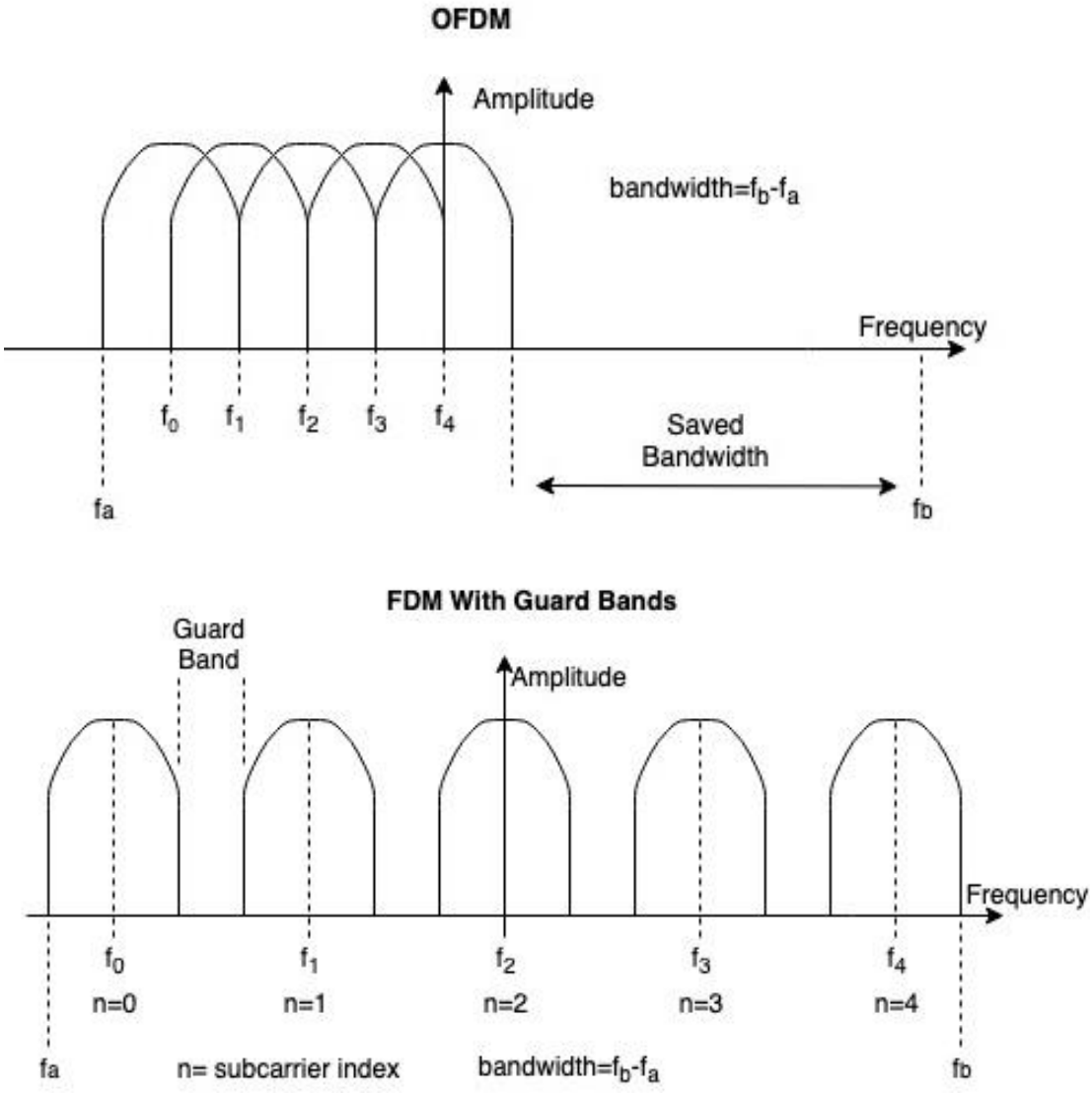


Figure 5- FDM vs OFDM Bandwidth Use Comparison

Orthogonality brings with it three main benefits [9]:

1: Complex filters, which are required at the transmitter and receiver in traditional FDM techniques, are not required.

2: It allows for digital signal processing (DSP) techniques to be taken advantage of such as the IFFT at the transmitter and the FFT at the receiver. Today FFT and IFFT system on chip (SOC) designs are readily available, of low cost and offer increasingly low power consumption.

3: Bandwidth efficiency is increased. Orthogonality enables more subcarriers to be used for a set bandwidth thus the available bandwidth is used much more efficiently. This is an especially important factor in the UWA channel where bandwidth is limited. Figure 5 shows how OFDM allows for bandwidth to be saved compared to FDM.

OFDM systems require very accurately synchronized transmitter and receivers. Any frequency offset e.g. Doppler spread, can result in a loss of orthogonality and ICI. Equation 11 shows the condition that must be met in order to maintain orthogonality between subcarriers.

$$\int_0^{T_b} \cos(2\pi nFt) \cdot \cos(2\pi kFt)\, dt = 0$$

Equation 11

Where $T_b$ is the symbol period, $n$ and $k$ are integers and $F$ is the fundamental frequency equal to $1/T_b$. Each $cos$ term denotes a different subcarrier being tested for orthogonality.

### 3.2.2 MODULATION

OFDM systems typically employ Quadrature Amplitude Modulation (QAM) and Phase Shift Keying (PSK) to map the inputted data bits to their symbols. QAM, as its name suggests, transmits data by varying the amplitude of the transmitted signal. Alternatively, PSK maps the inputted bits to symbols by modulating the phase of the transmitted signal.

Figure X shows the constellation mapping diagrams for the three modulation schemes employed in new OFDM technologies such as LTE [6]

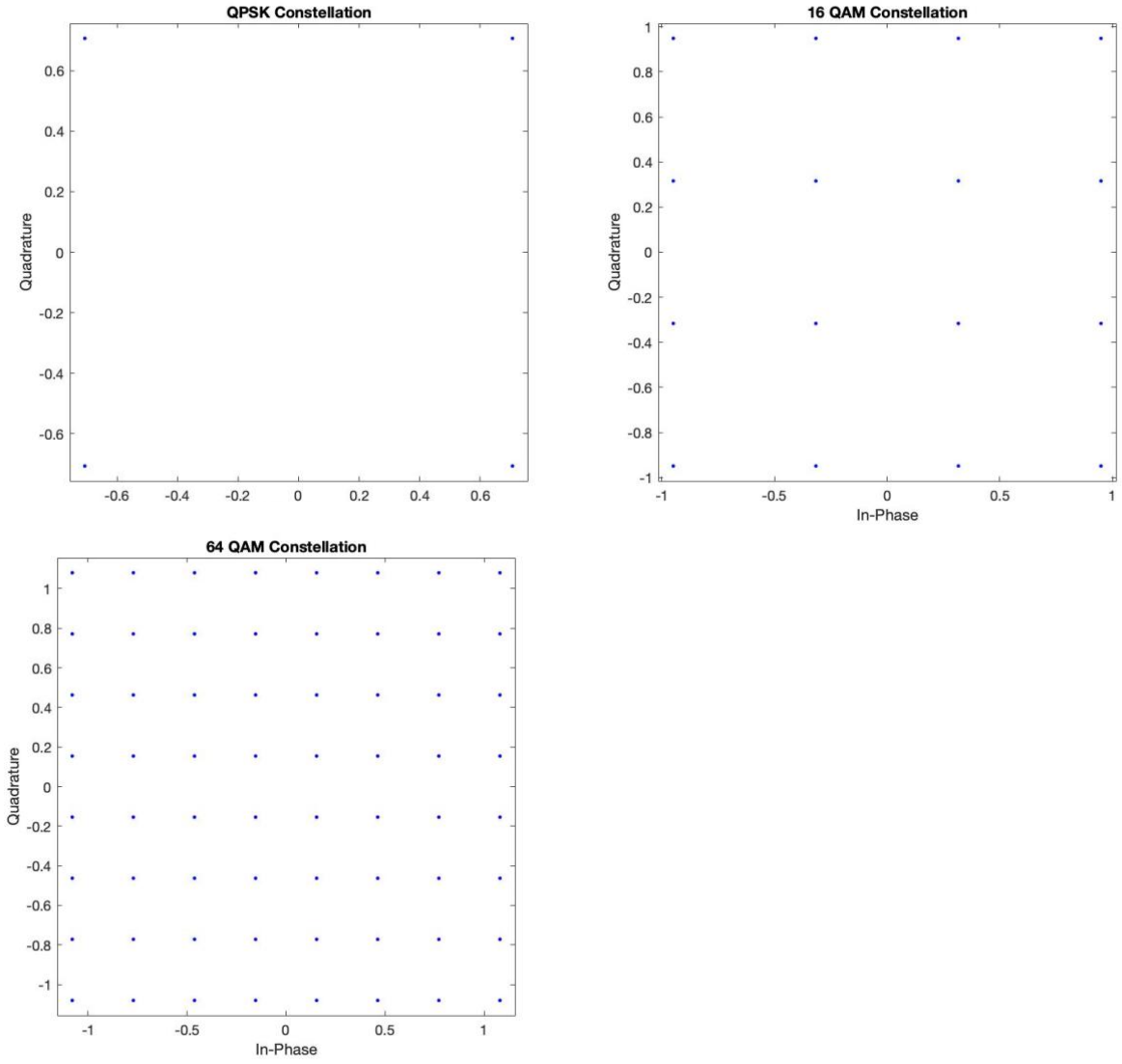


Figure 6- Constellation Mapping for QPSK, 16QAM and 64QAM

### 3.2.3 FFT

Without the use of FFT/ IFFT techniques the transmitter would require one oscillator per subcarrier to produce the baseband OFDM signal to be transmitted. With many orthogonal

subcarriers used this would be extremely high cost for hardware implementation [14]. For example, LTE employs 2048 subcarriers for a bandwidth of 20MHz [16].

Provided conditions are met for orthogonality to be maintained between all subcarriers digital signal processing (DSP) techniques such as IFFT at the transmitter and FFT at the receiver can be used. IFFT is used to convert the OFDM signal from the frequency domain to the time domain, and vice versa at the receiver for FFT.

### 3.2.4 GUARD INTERVAL

The popularity of OFDM in industry is due to its robustness against ISI. ISI is caused by multipath propagation and results in one OFDM symbol interfering with the next. If significant and not prevented, ISI can cause significant performance degradation [4]. OFDM prevents ISI by the addition of a guard interval at the end of each OFDM symbol, prior to transmission. The guard interval extends the symbol period by $T_g$, as shown in Equation 12. There are 2 types of guard interval used; cyclic prefix (CP) and zero-padding (ZP) [4].

$$T = T_b + T_g$$

$$T_b = \frac{1}{\Delta f}$$

Equation 12

where $T_b$ is the original symbol period, $T_g$ is the guard interval time period and $\Delta f$ is the frequency spacing between subcarriers.

In OFDM-CP, the last n samples of each OFDM symbol are copied and added to the front of the symbol, filling the guard interval and thus extending its time period by $T_g$. At the receiver the CP is removed since its samples are subject to interference.

In OFDM-ZP the guard interval is zero padded with no signal transmitted [18]. At the receiver there is no need to remove the zero padded part of the symbol as the FFT is only

computed over the time period $T_b$. In channels with a very large delay spread ZP offers better power efficiency.

It is possible to completely remove ISI provided the guard interval $T_g$ is larger than the maximum delay spread of the channel. In industry, the guard interval is typically defined as a fraction of the original symbol period $T_b$ . An example of this is DVB-T standard, which employs guard intervals of either 1/32, 1/16, 1/8 or 1/4 of the symbol period [19]. A further benefit from the introduction of a guard interval is that it reduces the transmitter- receiver pair's sensitivity to time synchronization problems. The spectral efficiency of OFDM is shown to be:

$$S(\%) = \frac{T_b}{T_b + T_g} \cdot 100$$

Equation 13

### 3.2.5 EQUALISATION

Provided the number of subcarriers is high, OFDM can be seen to convert a wideband channel into many narrowband sub-channels (subcarriers). This means that each subcarrier experiences flat fading even in a frequency selective channel. This allows for simple equalisation methods to be used to undo the effects of channel distortion. Two equalisation methods common in literature are discussed here.

#### ZERO FORCING

OFDM allows for the implementation of simple frequency domain zero forcing (ZF) equalisation. This is required to undo the frequency selective nature of the channel, and any distortion this can introduce.

It is known that for a noise free received signal $Y(f)$, an estimate of the transmitted signal $\hat{X}(f)$ can be made by simple division by the estimated channel transfer function $\hat{H}(f)$.

$$\hat{X}(f) = \frac{Y(f)}{\hat{H}(f)}$$

Equation 14

The channel's transfer function can be estimated with the introduction of pilot subcarriers. Known information is symbol mapped and transmitted on each pilot subcarrier. Since the receiver knows the information transmitted it can produce an estimation of the channel response for each pilot subcarrier, using Equation 14. It is then possible to interpolate the channel responses calculated, such that an estimate for the channel response across all subcarriers is formed [20]. The received symbol set can then be divided by the channel responses for the set of N subcarriers, such that the transmitted symbols are recovered. Pilot subcarriers can be arranged in a variety of formations as shown in figure X below.

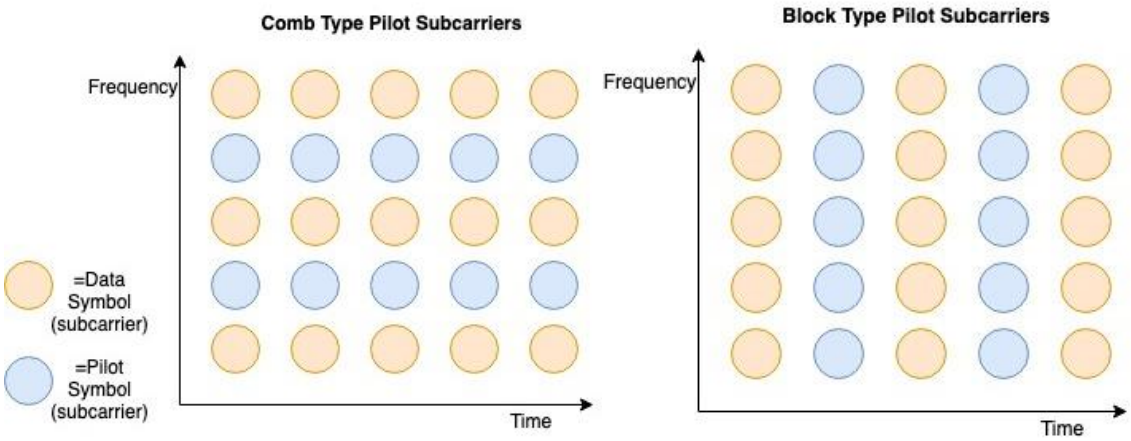


Figure 7- Comb and Block Type Pilot Subcarrier Arrangements

In a noise free environment ZF equalisation can provide perfect symbol recovery, however this is not practical. Noise amplification can occur for particularly deep fades where the estimated channel response can tend to 0 [21].This is shown in Equation 15. It's important to note that this only occurs in channels with significant distortion such that deep fading occurs.

$$\hat{X}(f) = \frac{Y(f)}{\hat{H}(f)} + \frac{N(f)}{\hat{H}(f)}$$

Equation 15

**MMSE**

Another equalisation method employed with OFDM is minimum mean squared error (MMSE). It makes use of the signals SNR to determine when deep fades occur. At high SNR

values it functions as a ZF equaliser however at low values of SNR it ensures noise amplification is limited. Equation 16, shows the MMSE equaliser equation, which is very similar to that of the ZF equation, but with the addition of noise factor $\frac{\sigma_n^2}{\sigma_s^2}$ [9].

$$\hat{X}(f) = \frac{\hat{H}^*(f)}{\left|\hat{H}(f)\right| + \frac{\sigma_n^2}{\sigma_s^2}} \cdot Y(f)$$

Equation 16

### 3.3 FEC CODES

Forward error correction (FEC) coding is important in OFDM to compensate for the bit errors that a fading channel can introduce. This is especially relevant in an UWAC where there is typically a high level of background noise.

FEC coding adds redundant information to the transmitted signal to enable the decoder to detect and then correct any errors without the need for retransmission methods such as automatic repeat request (ARQ) [9]. The addition of redundant data obviously reduces the spectral efficiency associated with a transmitted signal, as less useful data is throughput, but can bring with it large coding gains and potentially higher data rates if sufficient bandwidth is available.

The information theory behind powerful FEC codes has been around for a long while however the hardware technology available to turn theory into reality has been limited. In industry a wide range of FEC codes have been implemented within OFDM system structures. Half rate convolutional codes are used within Wi-Fi standards such as 802.11a [1], with more powerful turbo and low density parity check (LDPC) codes being introduced in newer LTE and DVB-S2 standards. More powerful codes tend to come with increased complexity but work only a few tenths of a decimal from the Shannon limit [22].

#### 3.3.1 CONVOLUTIONAL CODES

Before the first paper on turbo codes in 1993 convolutional codes were the class of codes that operated closest to the Shannon limit. A convolutional encoder consists of a finite set of shift

registers with the outputted code formed from linear combination of the shift registers value [23]. Each inputted bit results in the encoder changing state, with the number of states being equal to $2^v$ with v equal to the number of shift registers. Figure 8 shows the standard 64 state ½ rate encoder used in 802.11a Wi-Fi [1].

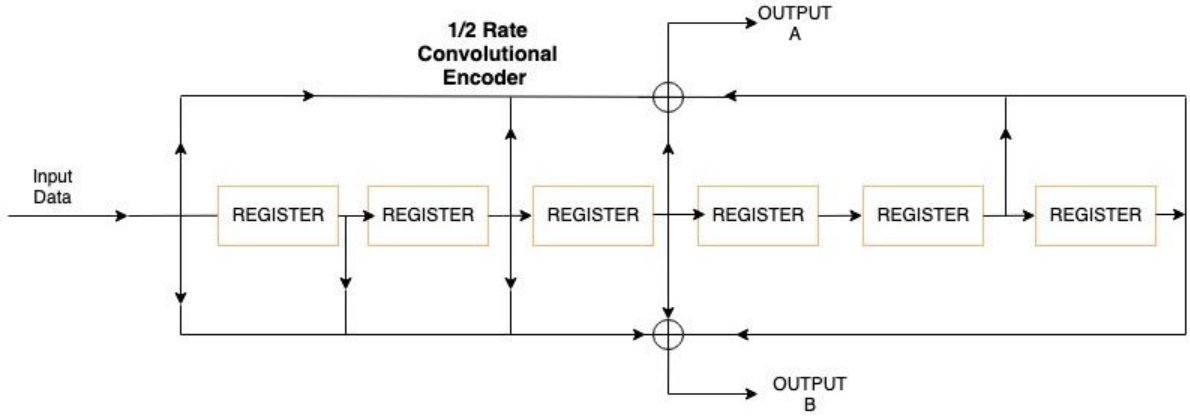


Figure 8- 64 State 1/2 Rate Convolutional Encoder

Equation 17 shows the code rate $R$ associated with n outputted bits for an inputted bit stream of length k.

$$R = \frac{k}{n}$$

Equation 17

Convolutional decoders use the Viterbi decoding algorithm. Each decoder is fed with either hard or soft inputted data, after which it makes a maximum likelihood (ML) estimate of the encoded data based upon finding the shortest path on a trellis graph. The shortest path can be defined in several ways. With soft inputted data the shortest path is defined by the Euclidean distance yet with hard inputted data, the shortest path is defined in terms of Hamming distance [23]. It is known that soft decision decoding outperforms hard decision decoding, however soft decision decoding is more complex.

### 3.3.2 TURBO CODES

Turbo codes are built upon 2 parallel recursive systematic convolutional (RSC) encoders separated by a random interleaver. Aside from outperforming convolutional codes at lower

SNRs, RSC codes resemble random codes. According to Shannon it is this factor that makes them so powerful since 'random-like codes are the key to approaching capacity' [22]. The architecture of each RSC encoder used can vary depending on the number of states and encoding/decoding complexities required. Figure 9 shows the standard architecture of a classical 1/3 rate turbo encoder. It is common to use puncturing techniques in conjunction with turbo codes. Puncturing allows for higher rate codes to be produced from lower rate codes with the omission of some data [24]. For example, omitting 2 out of every 6 bits outputted from the classical 1/3 rate turbo encoder will result in a greater code rate of ½ at the cost of a weaker code.

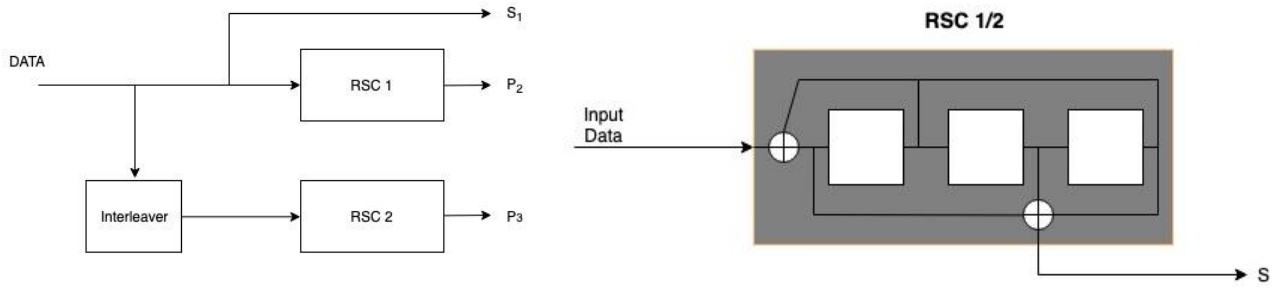


Figure 9- 1/3 Rate Turbo Encoder Architecture

Turbo decoding relies upon an iterative decoding strategy between two soft input soft output decoders [25]. Each decoder computes the probabilities of each bit being either a 1 or 0 in the form of a log likelihood ratio (LLR) denoted by Equation 18. The decoder pair updates the LLR information each iteration, until both decoders converge on a stable decision.

$$L(d) = \ln\left(\frac{\mathrm{P}\{d=1\}}{1-\mathrm{P}\{d=1\}}\right)$$

Equation 18

where $\mathrm{P}\{d = 1\}$ is the probability that the binary datum has value 1 at a point in the decoding strategy. The sign of $L(d)$ gives the hard decision of d. $|L(d)|$ gives reliability of this decision [22].

With puncturing often used, it is important to note that the decoder has no information on the omitted (punctured) data bits. All the decoder knows is the relevant locations at which data bits have been omitted. At these locations, it de-punctures the data bits by setting their LLR to 0. This is equivalent to setting equal probability of the data bit being a 1 or 0.

### 3.3.3 LDPC

LDPC codes are a type of linear block code of fixed length used within standards such as DVB-S2 [17]. LDPC codes offer significant coding gain and are encoded in 2 steps. At first a sparse parity check matrix H is formed. Then, by mathematical analysis, the generator matrix G can be formed. Code-words can then be generated by a simple multiplication of the inputted data by G [26].

Similar to turbo codes, LDPC codes are decoded using an iterative decoding algorithm. A variety of decoding algorithms can be used such as MAP or SOVA [26] [27].

## 3.4 OFDM TRANSMISSION

The OFDM transmitters block diagram is shown below. It clarifies the order in which the fundamental OFDM steps of section 3.2 are taken.

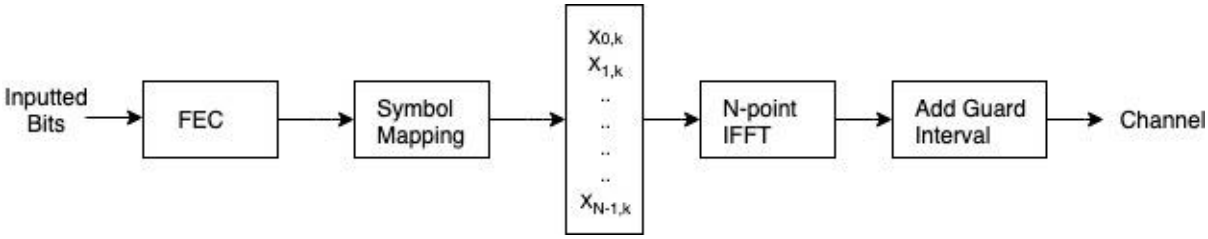


Figure 10- OFDM Transmitter Block Diagram

The inputted bits are first encoded using the FEC code of choice after which the encoded data is symbol mapped onto each subcarrier. The N point IFFT transform of the symbol set is then computed, converting the frequency domain signal to its time domain equivalent. Once in the time domain, a guard interval is inserted, extending the symbol period by $T_g$ prior to transmission.

### 3.6 OFDM RECEIVER

The OFDM receivers block diagram is shown below. The first step taken at the receiver is to remove the guard interval of the received signal, since this contains interference. The frequency domain equivalent of the received signal is then recovered via N point FFT, after which equalisation takes place to reverse the effects of channel distortion. Following on from this each symbol is demodulated and then decoded, with the received data bits being outputted.

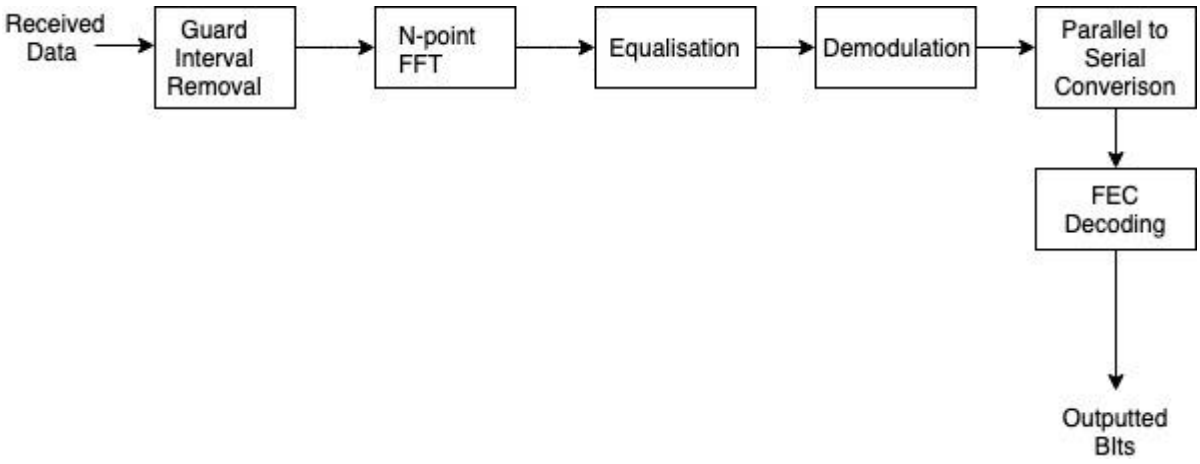


Figure 11- OFDM Receiver Block Diagram

The throughput of OFDM system is equal to:

$$D_{Th} = R \cdot \frac{N}{T_b + T_g} \cdot k$$

Equation 19

where $R$ is the code rate, $N$ is the number of subcarriers, $T_b + T_g$ is the symbol period and $k$ is the number of bits per symbol. $k = \log_2 M$ , where $M$is the constellation size.

### 3.7 PROBLEMS WITH OFDM IN THE UWAC

OFDM's robustness against ISI along with its effective use of bandwidth makes it a popular choice for open air radio transmission. Despite this, several problems are associated with OFDM in the UWAC. These are summarised below:

- The large Doppler spread in the UWA channel can cause uncorrelated frequency shifts across all the subcarriers. If uncorrected, this will cause a loss of orthogonality between subcarriers, resulting in severe ICI. Doppler estimation algorithms/ techniques are therefore necessary to undo the effects of the frequency selective nature of the channel.

- Although OFDM effectively uses the bandwidth available, the addition of a guard interval limits the achievable bit rate. In a bandwidth limited channel, such as the UWA channel, this is far from ideal since high data rates will be difficult to achieve.

# CHAPTER 4

# ORTHOGONAL FREQUENCY DIVISION MULTIPLEXING OFFSET-QAM

In 1967, 2 years after Chang's original OFDM proposal, Saltzberg introduced an OFDM system with two sets of integrated filter banks [28]. He concluded that with filter banks a significant improvement to the pulse shaping of each subcarrier could be made with less out of band leakage. Hirosaki extended Saltzberg's work with the implementation of DSP techniques such as the discrete Fourier transform (DFT). He determined that OFDM-OQAM offered significantly better performance than single carrier (SCM) techniques. Since then the majority of research has been concentrated on developing pulse shaped filters that are well localized in the frequency and time domain. An example of this is the PHYDAS project which looked into the development of the OFDM-OQAM physical layer for future wireless technologies [29]. On the back of this OFDM-OQAM is a candidate for new 5G technologies as it offers benefits over traditional OFDM-CP such as improved spectral efficiency and resilience against Doppler spread [30].

This chapter begins with a general overview of OFDM-OQAM followed by a more detailed analysis of the OFDM-OQAM pre-processing operation and filter banks. A range of prototype filters from literature are then discussed.

## 4.1 OFDM-OQAM GENERAL DESCRIPTION

OFDM-OQAM, also known as filter bank multi carrier (FBMC), can be seen as a substitute for traditional OFDM-CP that offers improved spectral efficiency due to the absence of the cyclic prefix [30]. OFDM-OQAM introduces a pair of filter banks with a synthesis filter bank (SFB) at the transmitter and an analysis filter bank (AFB) at the receiver. A complex to real symbol operation, followed by the staggering of real and imaginary parts by half a symbol period allows for pulse filters well localized in frequency and time to be used, while ensuring maximum spectral efficiency is maintained [31]. Extensive research into the feasibility of OFDM-OQAM for future wireless technologies and UWA communications has yielded two methods for OFDM-OQAM implementation. They are known as the frequency spreading (FS) method and the polyphase network (PPN) method. In this thesis the PPN method will be

selected due to its ease of implementation without the need for additional filtering operations [31].

## 4.2 OQAM PRE-PROCESSING

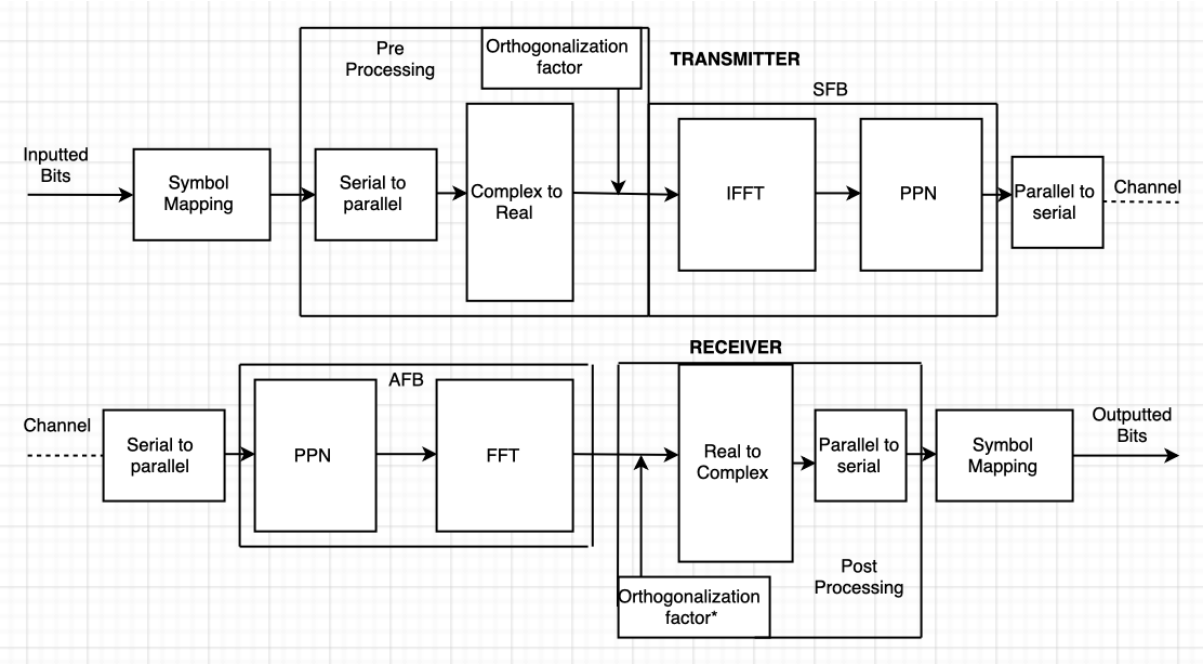


Figure 12- OFDM-OQAM System Diagram

Figure 12 shows the subsystem diagram for OFDM-OQAM. The OQAM pre-processing operation begins with mapping the inputted bit stream to the relevant QAM symbols as completed in traditional OFDM-CP. Each QAM symbol then goes about a complex to real conversion resulting in each symbol $S_{k,i}$ being split into its real and imaginary parts, as shown in equation 1.

$$S_{k,i} = c + bj\,, \qquad 0 \leq k \leq K-1$$

$$a_{k,(n-1)} = \Re\{S_{k,i}\} = c$$

$$a_{k,n} = \Im\{S_{k,i}\} = b$$

Equation 20

where $k$ is the subcarrier index, $K$ is the total number of subcarriers, $i$ is the initial sample index and $n$ is the new sample index after up sampling. Nb. $n = 2i$

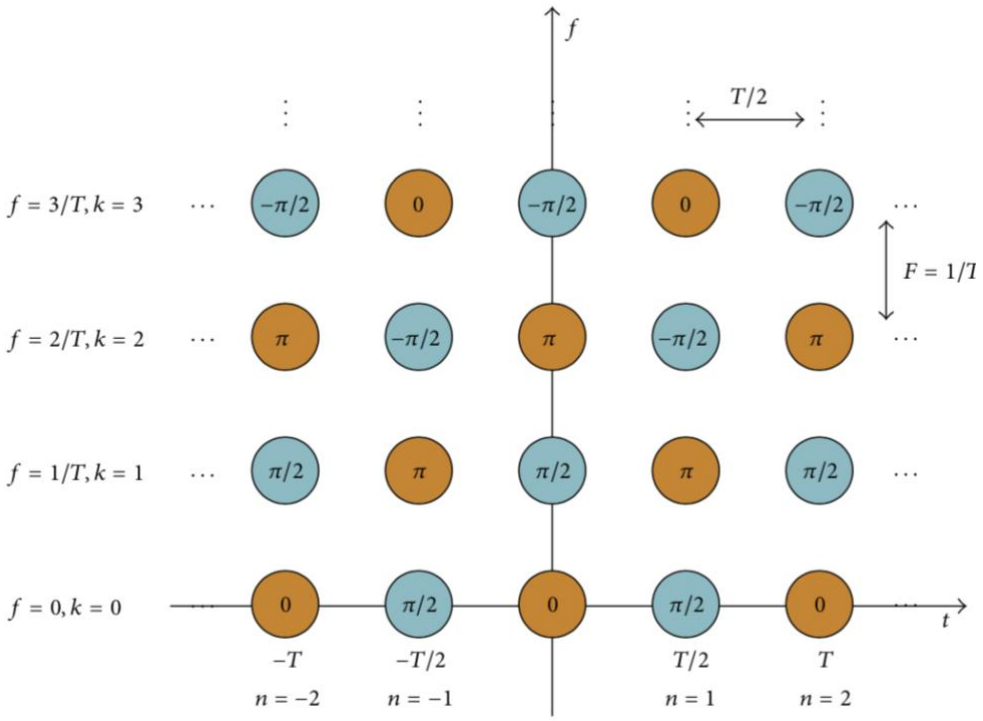


Figure 13- Pre Processing Output

It is to be noted that the real and imaginary part of each symbol is separated by half a symbol duration $\frac{T}{2}$ thus increasing the sampling rate by a factor of 2. This delay of half a symbol period is administered by each subcarrier's pulse shaped filter which is shifted in time. In addition to this the separated imaginary and real parts of each symbol are multiplied by an orthogonalization factor θ, which results in a phase offset of $\frac{\pi}{2}$ between adjacent symbols along the frequency and time axes of Figure 13.

$$\theta_{k,n} = e^{j(k+n)\frac{\pi}{2}} = j^{k+n}$$

Equation 21

where k is the subcarrier index, and n is the sample index at the pre-processing output.

This ensures orthogonality is maintained between the terms $a_{k,(n-1)}$and $a_{k,n}$ and adjacent subcarriers prior to entering the SFB. Despite this orthogonality must be relaxed to only the real field after leaving the SFB. This is because the filter bank consists of a set of purely real prototype filters which according to Balian's theory cannot be well localized in time and frequency, maintain complex orthogonality and achieve maximum spectral efficiency.

After multiplication by the orthogonalization factor θ the IFFT of each sample set is computed, converting the signal from the frequency domain to its discrete time domain equivalent $Xp[n]$ represented in equation 22.

$$Xp[l] = \theta_{k,n} \cdot a_{k,n}$$

$$Xp[n] = \mathcal{F}^{-1}\{Xp[l]\} = \frac{1}{\sqrt{K}} \sum_{k}^{K-1} Xp[i] e^{j2\pi nk/K}$$

Equation 22

### 4.3 SYNTHESIS FILTER BANK

The symbols on each subcarrier are then passed through the synthesis filter bank as shown in figure X. The filter bank is an array of filters equal to the number of subcarriers. It is designed from a prototype filter to specifically produce a well localized sub channel in the frequency and time domain [29]. This enables ICI and ISI to be efficiently reduced without the need of a cyclic prefix. Figure X shows an example of the frequency response of the filter bank compared to the frequency response of traditional OFDM-CP systems. It can be seen that the filter bank has better frequency selectivity and thus very limited out of band leakage compared to OFDM-CP.

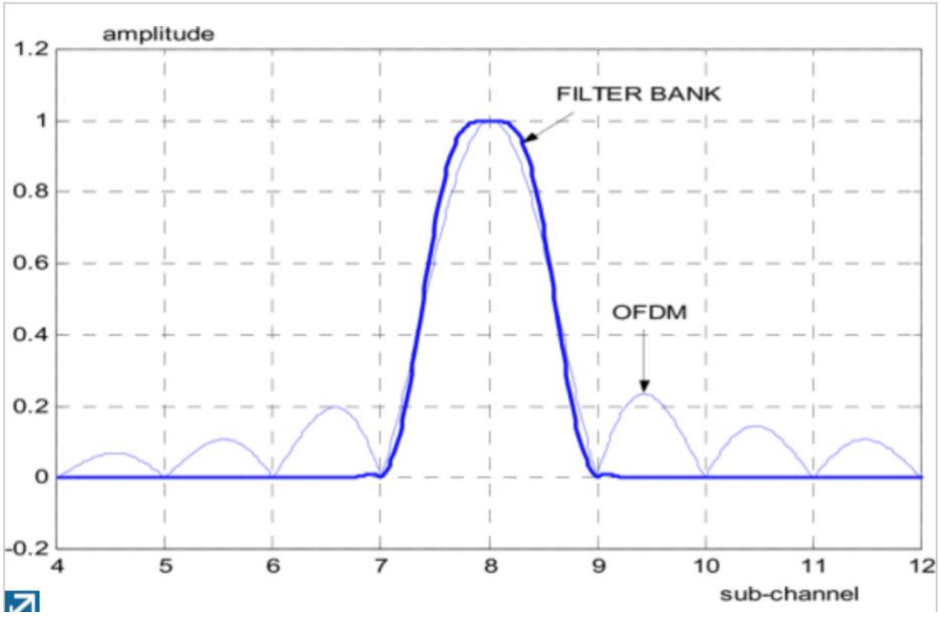


Figure 14- Frequency Response of Filter Bank Compared to OFDM-CP [SOURCE *[29]*]

SFB design begins with the selection of a prototype filter which is then extended across the entire bandwidth with frequency shifts [32]. This forms K filters with each single filter centred on one subchannel. It can be seen in figure X that even or odd subcarriers do not overlap, such that subcarriers are only affected by their neighbouring subcarriers. OQAM modulation allows for orthogonality between adjacent channels to be maintained as in each subchannel only the real or imaginary part is transmitted. This prevents ICI between adjacent subchannels. Alternatively, OFDM-CP requires orthogonality to be maintained between all subcarriers.

If standard QAM modulation was instead used, orthogonality would not be maintained between neighbouring subcarriers and there would be significant ICI. To combat this, only odd (or even) subcarriers could be used for data transmission, such that there would be no overlap in the frequency domain, however this would result in the bit rate being reduced by half along with half the capacity being unused.

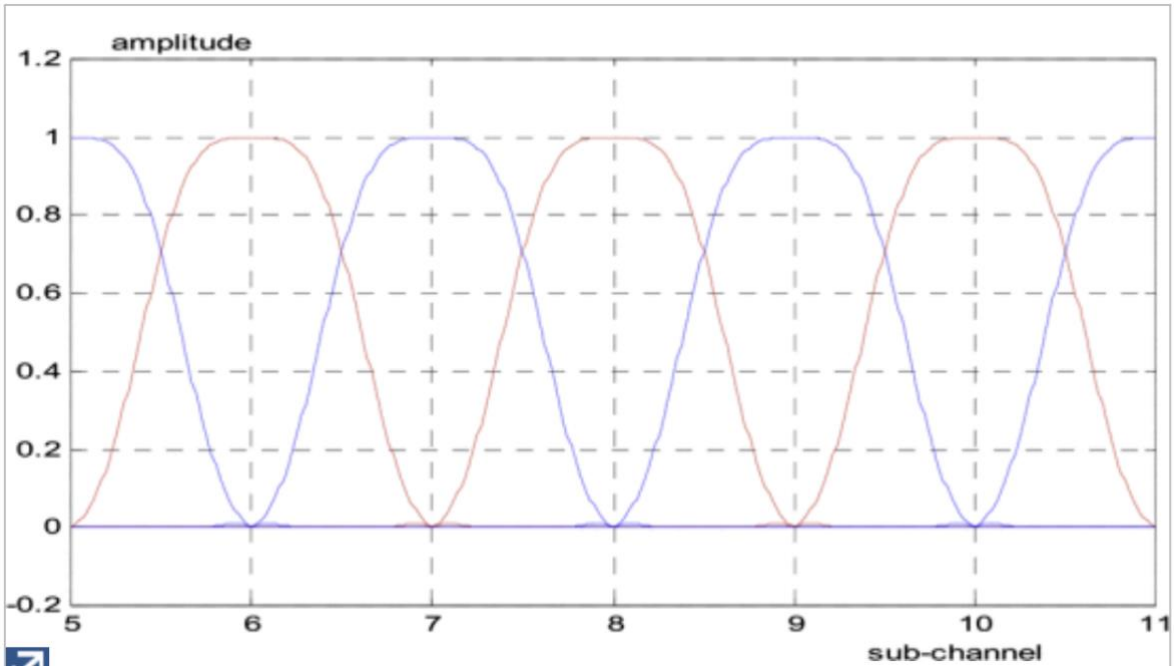


Figure 15- SFB Frequency Response [SOURCE *[29]*]

## 4.4 PROTOTYPE FILTERS

A variety of prototype filters have been proposed for OFDM-OQAM systems such as the PHYDAS and IOTA. Prototype filters are designed with several parameters in mind including energy distribution in the time domain and a sharp frequency response in the frequency domain. They are characterised by an overlapping factor p, which is equal to the ratio of the filter length L over the number of subcarriers K. This factor is equal to the number of symbols that overlap one another in the time domain.

It is known that the filters must follow the Nyquist theory such that the impulse response crosses the zero axis at all integer multiples of the symbol period. Alternatively, in the frequency domain this corresponds to a filter with symmetry about the cut off frequency. There are typically two methods for filter design; the frequency spreading method and the window based technique [32]. In the former method the impulse response of the filter is obtained by taking samples of the IFFT of the desired frequency response. The latter method involves multiplying a window function by a low pass filter to obtain the prototype filter.

### 4.4.1 PHYDAS FILTER

The prototype PHYDAS filter was first designed by Bellanger in [29] His work was further developed in the multi million pound PHYDAS research project of 2010 which looked into the development of FBMC physical layer for future efficient wireless and mobile radio networks. It proposed the use of a finite impulse response (FIR) filter for FBMC systems.

Table X shows the frequency domain coefficients of the PHYDAS filter for different values of overlapping factor p. In this thesis p will be assumed to be 4, since this value has been shown to produce a high frequency selective filter in [29] and [31]. For an overlapping factor of 4 the filter has frequency domain coefficients equal to:

$$P_0 = 1, \qquad P_{\pm 1} = 0.97196, \qquad P_{\pm 2} = {\sqrt{2}}/{2}, \qquad P_{\pm 3} = 0.235147$$

| $p$ | $P_0$ | $P_1$ | $P_2$ | $P_3$ | $\sigma^2$ |
|---|---|---|---|---|---|
| **2** | 1 | $\sqrt{2}/_2$ | - | - | -35 |
| **3** | 1 | 0.911438 | 0.411438 | - | -44 |
| **4** | 1 | 0.971960 | $\sqrt{2}/_2$ | 0.235147 | -65 |

Table 2-PHYDAS Frequency Domain Coefficients

The frequency response $H(f)$ of the filter can be calculated using equation 23, and consists of 2p-1 pulses. It can be seen in figure 16 that this produces a highly frequency selective response with very little out of band leakage.

$$H(f) = \sum_{c=-(p-1)}^{p-1} P_c \frac{\sin(\pi\left(f - \frac{c}{Kp}\right)Kp)}{Kp \sin \pi\left(f - \frac{c}{Kp}\right)}$$

Equation 23

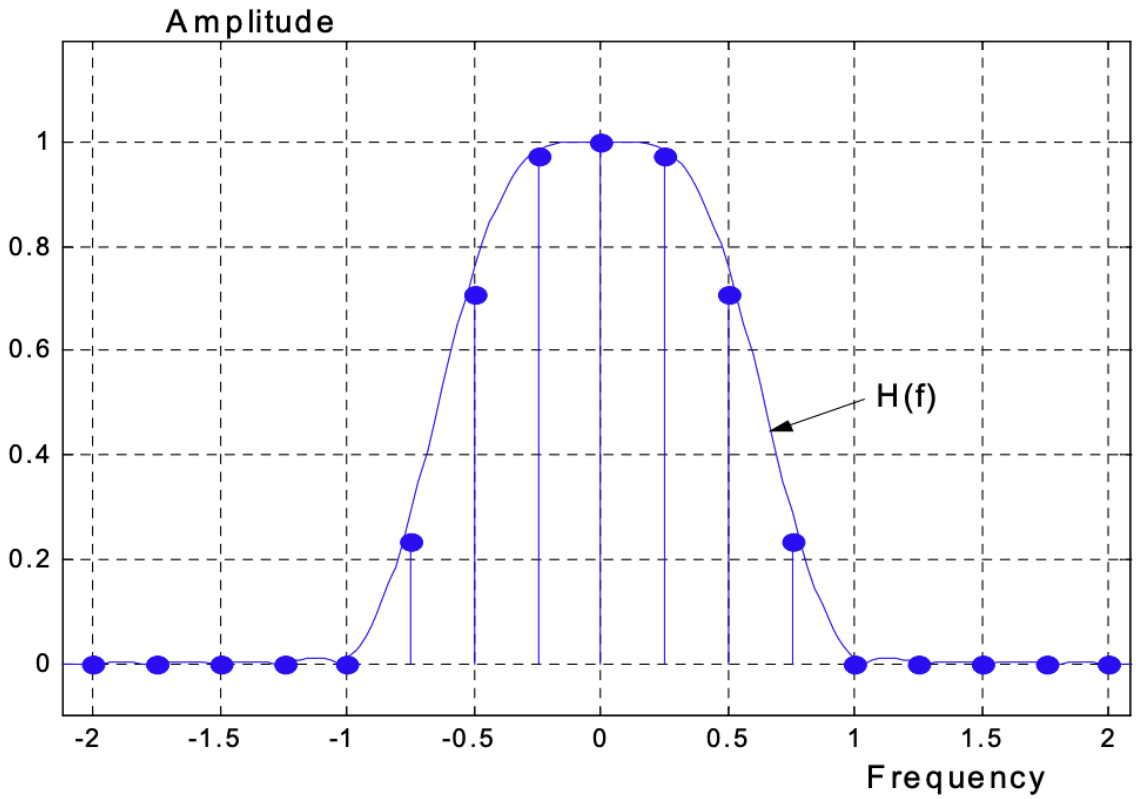


Figure 16- PHYDAS Filter Frequency Response [SOURCE [29]]

The impulse response of the filter can be derived by taking the IFFT of the frequency response $H(f)$. This is shown in Equation 24.

$$h[m] = 1 + 2\sum_{c=1}^{p-1} P_c \cos(2\pi \frac{cm}{pK}), \qquad 1 \leq m \leq L-1$$

$$h[0] = 0$$

Equation 24

where $L = pK$ is the filter's length and $h[0]$ is required to ensure that there is an odd number of coefficients. This allows for the delay of the filter to be an integer multiple of $T/2$. The impulse response of the filter is shown in Figure 17.

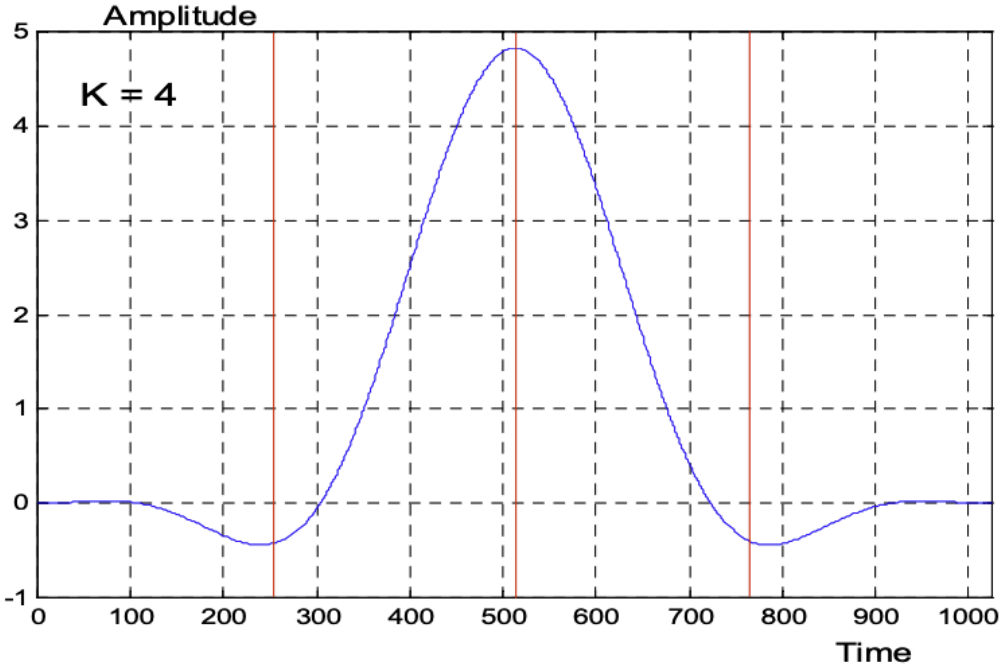


Figure 17-PHYDAS Filter Impulse Response [SOURCE [29]]

### 4.4.2 IOTA FILTER

The isotropic orthogonal transform algorithm (IOTA) filter is another prototype filter that has been developed specifically for OFDM-OQAM. It was patented by Alard and has recently found its way into 3GPP standards. The IOTA filter is formed by orthogonalizing the symmetric Gaussian function in time and frequency to avoid ISI and ICI.

## 4.5 ANALYSIS FILTER BANK

The received signal at the receiver is placed through an analysis filter bank (AFB). The AFB is a time reversed, complex conjugated version of the prototype filter, and works in much the same way as the SFB.

In a similar way to the SFB, the AFB is formed from frequency shifts of a prototype filter. The same prototype filter must be used for both the SFB and AFB such that the condition of equation 25 is met:

$$g(t) = g(-t)$$

Equation 25

## 4.6 OQAM POST PROCESSING

As shown in figure 12 the OQAM post processing operation is a reversal of the OQAM pre-processing operation. Each subcarrier's frequency domain signal, after equalisation, is multiplied by the complex conjugate of the orthogonalization factor of equation 21. This is followed by a real to complex operation where the separated real and imaginary parts of each symbol are added together.

## 4.7 EQUALISATION

Equalisation is crucial at the receiver to limit the effect of channel distortion upon overall system performance. More specifically it must be performed to reduce ISI between the separately transmitted real and imaginary parts in frequency selective channels. Provided the filter banks exhibit high frequency selectivity, along with each subcarrier being suitably

narrow such that it experiences flat fading, a single tap equaliser per subcarrier is sufficient. In frequency selective channels more complex equalisation methods must be used.

A wide variety of equalisation methods are discussed and simulated in X, including MMSE, simplified MMSE, multiband MMSE and frequency sampling equalizers. It concludes that MMSE and multiband MMSE outperform the other techniques in frequency selective channels. This is shown in figure 18.

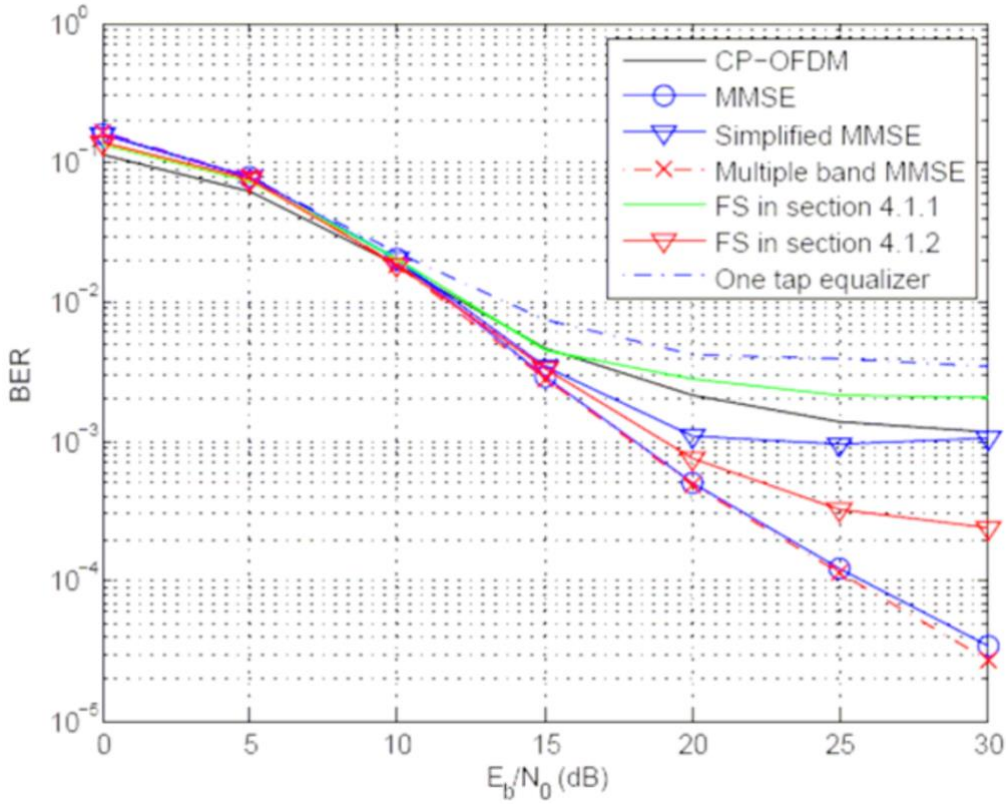


Figure 18-BER Performance of OFDM-OQAM Equalisation Methods [SOURCE [29]]

# CHAPTER 5

# EXPERIMENTAL RESULTS

This chapter contains an evaluation of the performance of both OFDM-CP and OFDM-OQAM systems simulated under various channel conditions. Section 1 begins with the analysis of each system's BER performance in additive white Gaussian noise (AWGN) and Rayleigh fading channels. This is followed by simulations in more realistic horizontal and vertical UWACs with FEC coding applied. In section 2 we evaluate the throughput performance of each system type. A short analysis of zero forcing equalisation then follows.

Each system was designed, built and simulated in MATLAB using the MATLAB communications toolbox. The toolbox enabled easy implementation of a variety of modulation schemes and FEC codes.

## 5.1 BER PERFORMANCE

### 5.1.1 BER PERFORMANCE IN AWGN AND RAYLEIGH FADING CHANNELS

The first experiment conducted evaluated the BER performance of each system in AWGN and Rayleigh fading channels. Each system operated with 2048 subcarriers over a bandwidth of 115KHz with a centre frequency of 97.5KHz. The cyclic prefix was set to ¼ of the original symbol length for the OFDM-CP system. For the AWGN channel, QPSK, 16 QAM and 64 QAM modulation schemes were tested, while only QPSK modulation was used in the Rayleigh fading channel.

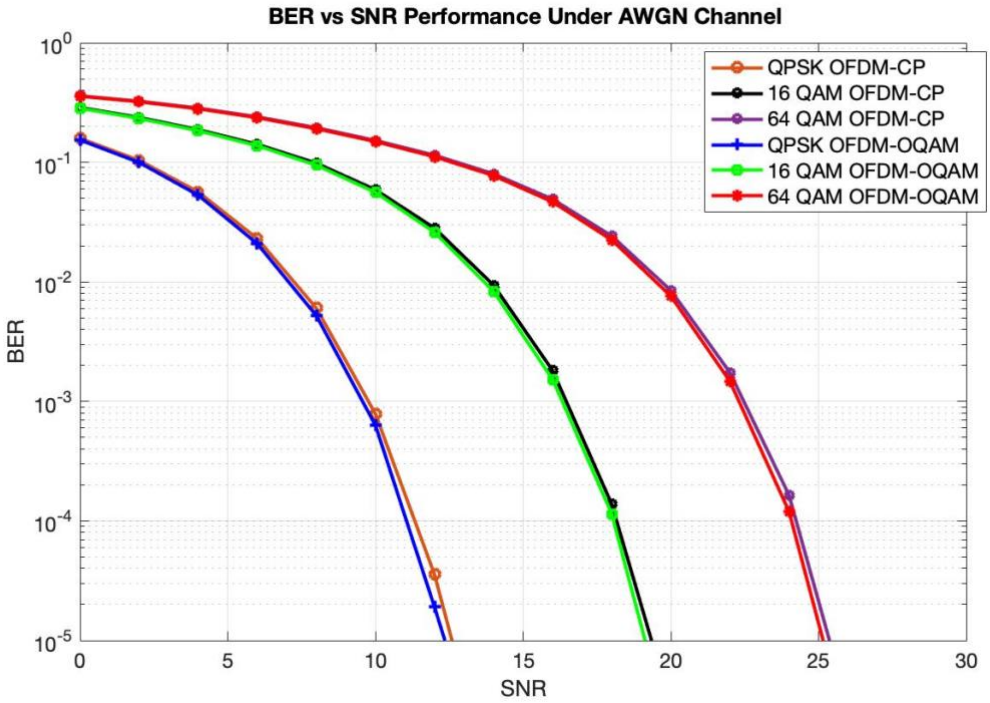


Figure 19-BER vs SNR (dB) in AWGN Channel

Figure 19 shows the simulation results of OFDM-CP and OFDM-OQAM in AWGN channel. In an AWGN channel the cyclic prefix has no effect on the performance of the system because there is no ISI. It is clear each system has identical BER performance for each modulation scheme used.

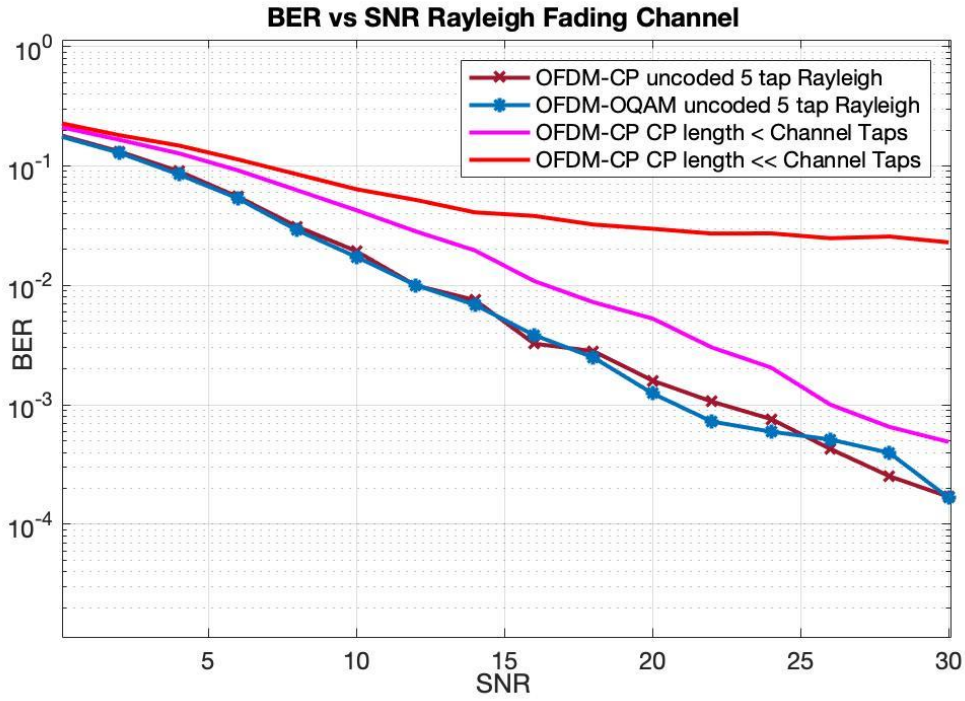


Figure 20-BER vs SNR (dB) Rayleigh Fading Channel

Figure 20 shows the BER performance of each system in a Rayleigh fading channel with zero forcing equalisation and perfect channel knowledge. OFDM-CP and OFDM-OQAM exhibit similar performance in a 5 tap Rayleigh fading channel with ISI perfectly removed. When the cyclic prefix length is smaller than the number of channel taps there is a noticeable drop in system performance because ISI isn't completely removed. Moreover, as the cyclic prefix length is reduced further it is apparent BER performance continues to degrade as ISI affects more symbols. This confirms that OFDM-CP requires a cyclic prefix to effectively remove ISI and maintain high performance.

### 5.1.2 BER PERFORMANCE IN THE VERTICAL AND HORIZONTAL UWACS

The second experiment tested each system's performance in realistic vertical and horizontal UWACs. Each channel applied frequency and distance dependent attenuation calculated using the Fisher and Simmons model. The vertical channel assumed single direct path transmission while the horizontal channel applied a significant delay spread due to multipath propagation. It is important to note that neither channel applied a Doppler spread to the transmitted signal since Doppler estimation methods are not considered in this research. For both vertical and horizontal channels, QPSK, 16 QAM and 64QAM modulation schemes were used with 8192 subcarriers over a bandwidth of 115KHz centred on a frequency of 97.5kKHz. This is summarised in table 4.

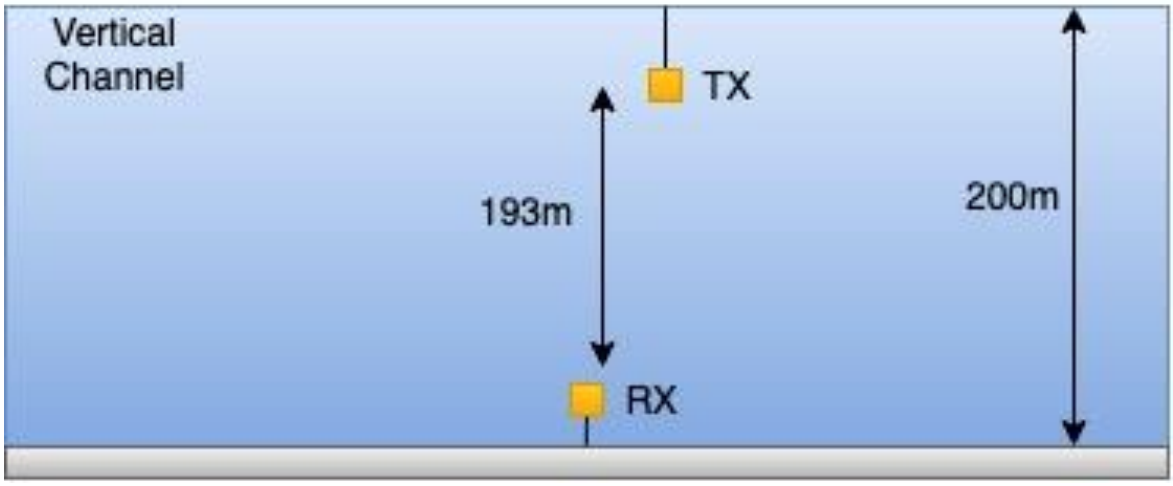


Figure 21- Vertical Channel Scenario

Figure 21 shows the transmitter – receiver setup for the vertical channel simulation. Transmission distance was set to 193m between a transmitter fixed at 2m depth and a receiver fixed at 195m depth. It is assumed that the channel has a depth of 200m. A complete list of channel parameters is shown in table 3.

| **Transmission Distance (metres)** | **Sea Depth (metres)** | **TX Depth** | **RX Depth** | **Salinity (PPT)** | **Temperature (°C)** | **pH** | **Spreading Factor** |
|---|---|---|---|---|---|---|---|
| 193 | 200 | 2 | 195 | 35 | 15 | 8 | 1.5 |

Table 3- Vert Channel Parameters

| **Number of Subcarriers** | **Bandwidth (KHz)** | **Centre Frequency (KHz)** | **$\Delta f$ (Hz)** | **Modulation Schemes** | **CP Length** |
|---|---|---|---|---|---|
| 8192 | 115 | 97.5 | 14.03 | QPSK, 16QAM, 64QAM | $1/4\,T_b$ |

Table 4- System Parameters

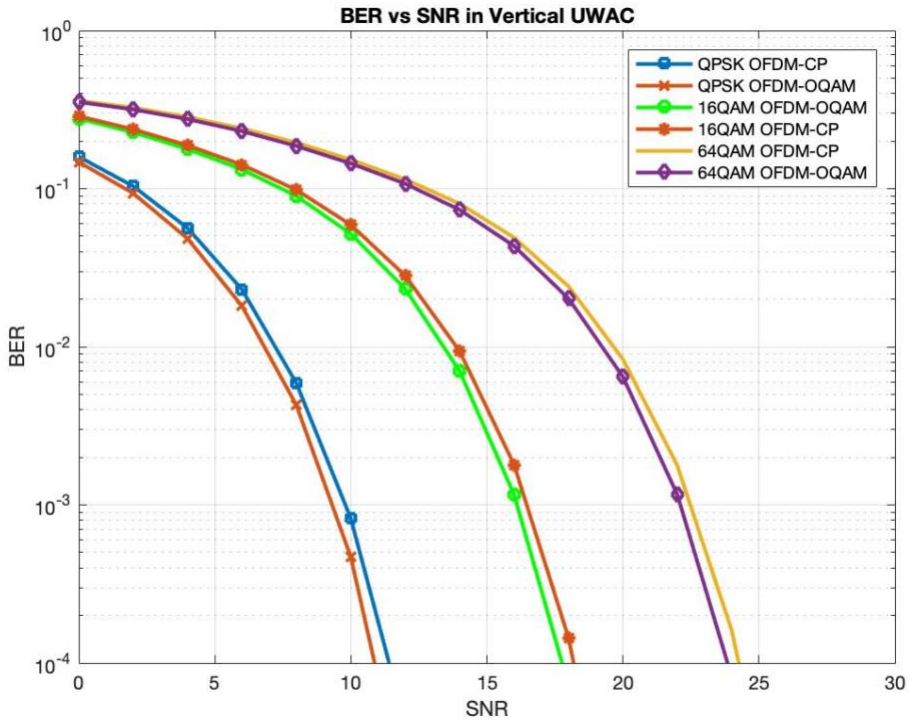


Figure 22-BER vs SNR (dB) Vertical UWAC

Figure X shows BER performance of OFDM-CP and OFDM-OQAM in a vertical UWAC. Since this channel assumes single path transmission it applies no delay spread to the transmitted signal and thus no ISI is present, resulting in very few bit errors. In fact, the BER performance approaches that of the AWGN channel in figure 19. It is clear OFDM-CP and OFDM-OQAM exhibit very similar BER performance for each modulation scheme. Moreover, the BER performance degrades as the modulation order is increased. This is because the constellation points of higher modulation orders are much closer together, such that for the same distortion, symbols of a higher modulation order are more likely to be incorrectly demodulated.

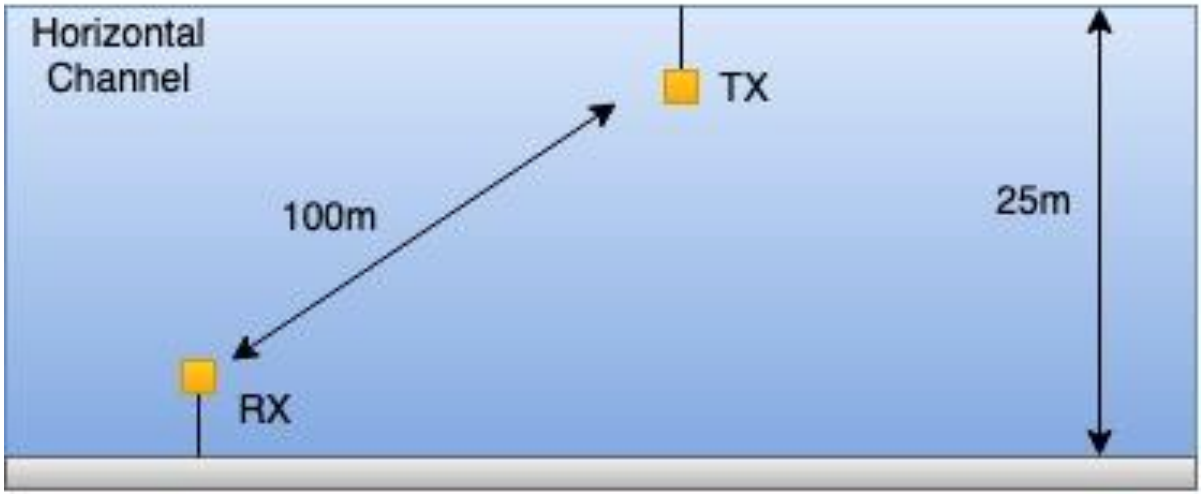


Figure 23- Horizontal Channel Scenario

Figure 23 shows the transmitter- receiver set up for the horizontal channel simulation. Transmission distance was set to 100m between a transmitter fixed at 2m depth and a receiver fixed at 20m depth. Channel depth was set to 25m while all other channel and system parameters, as shown in tables 3 and 4, were unchanged. Since this scenario is based upon a shallow horizontal UWA channel, there is significant multipath propagation resulting in a delay spread of 16.7ms as shown in figure 24.

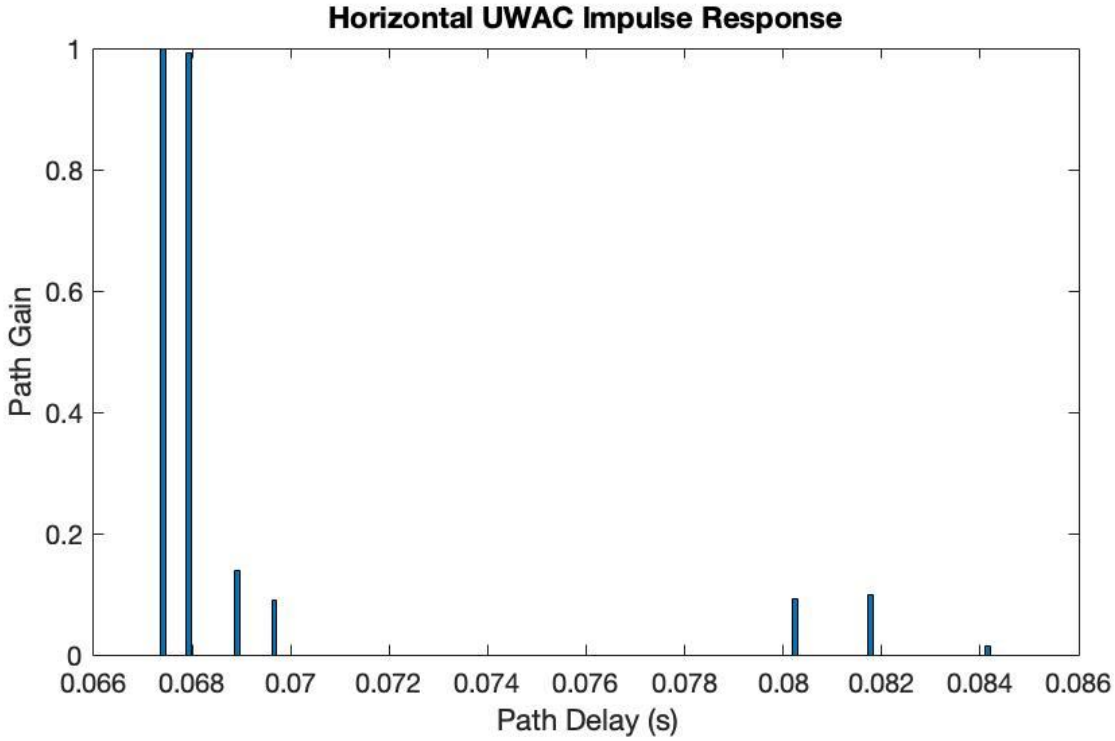


Figure 24-Horizontal Channel Impulse Response

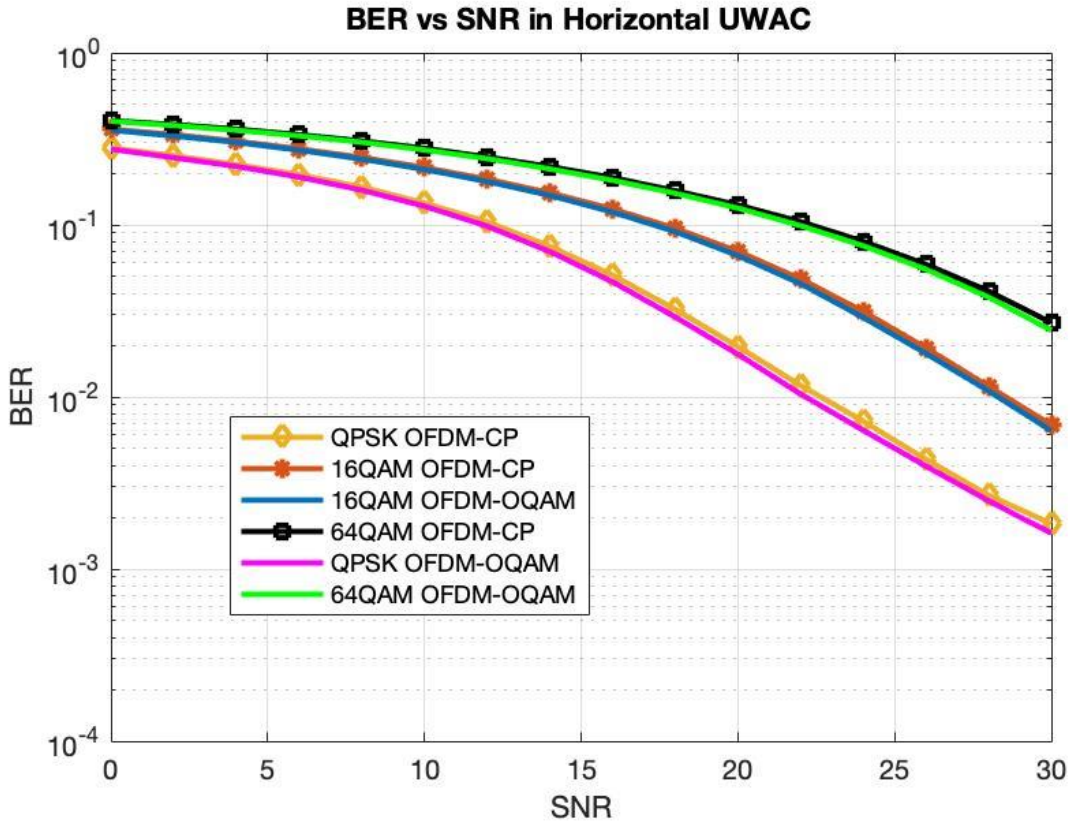


Figure 25- BER vs SNR (dB) Horizontal UWAC

It is clear that both OFDM-CP and OFDM-OQAM exhibit identical BER performance in this channel. Furthermore, each system suffers significantly more bit errors in this channel compared to the vertical UWAC. This is due to greater dispersion and attenuation as a result of multipath propagation in this channel. Moreover, the BER performance degraded as the modulation order was increased. This was also seen in the previous vertical UWAC simulation.

### 5.1.3 BER PERFORMANCE IN VERTICAL AND HORIZONTAL UWAC'S WITH FEC CODING

The third experiment investigated the performance of each system with a variety of FEC codes used. LDPC and turbo encoders and decoders were integrated into both OFDM-CP and OFDM-OQAM systems built within MATLAB. A range of puncturing patterns allowed for the code rate of each turbo encoder to be varied while MATLAB's inbuilt function ensured all LDPC code rates within the DVB-S2 standard could be used. The same vertical and horizontal channels as depicted in figures 21 and 23 were used. Only 16 QAM modulation was used however all other system parameters remained the same.

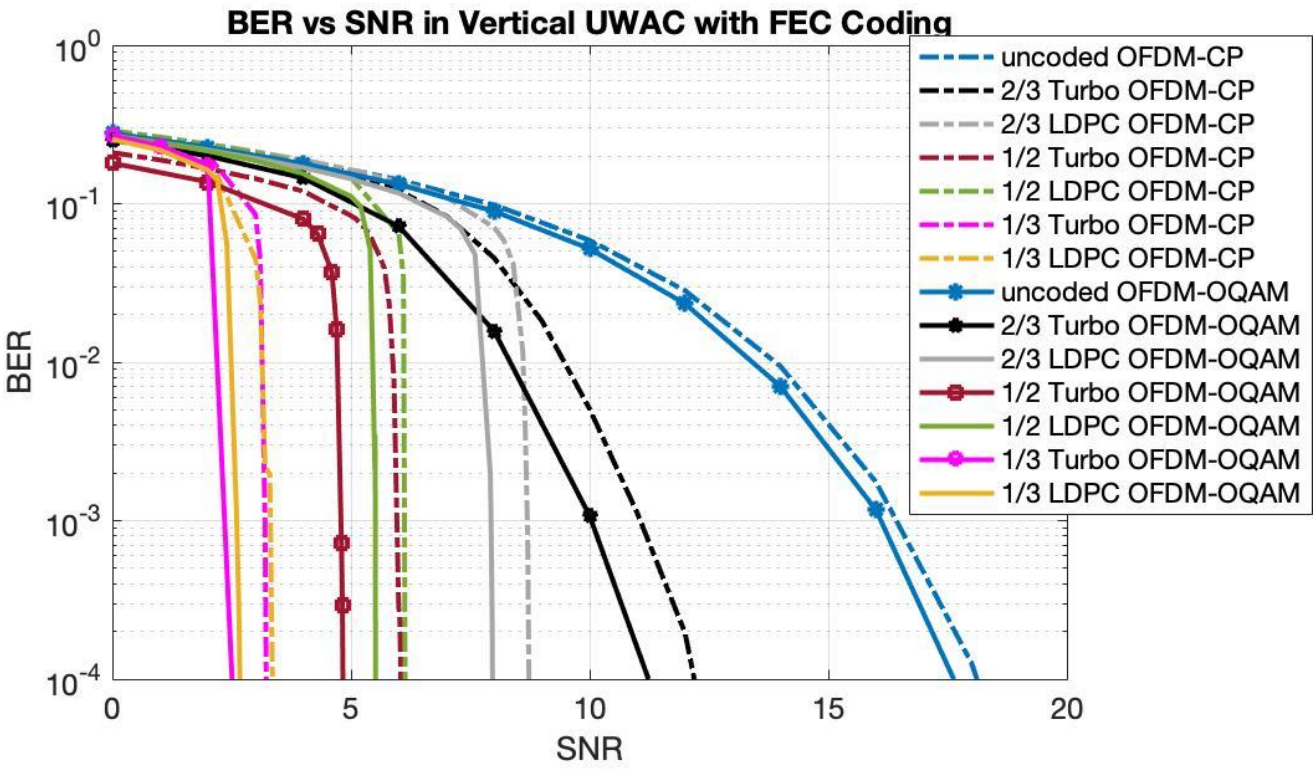


Figure 26- BER vs SNR (dB) in Vertical UWAC with FEC

Figure 27 shows the BER performance of each system with FEC coding in the vertical UWAC. FEC codes allow for significant coding gain, for instance at a BER of $10^{-3}$ OFDM-OQAM 1/3 rate turbo outperforms uncoded OFDM-OQAM by 13.5dB. It is also clear that coded OFDM-OQAM outperforms coded OFDM-CP for identical code type and code rate. For example ½ rate turbo OFDM-OQAM achieves 1.2dB coding gain over ½ rate turbo OFDM-CP.

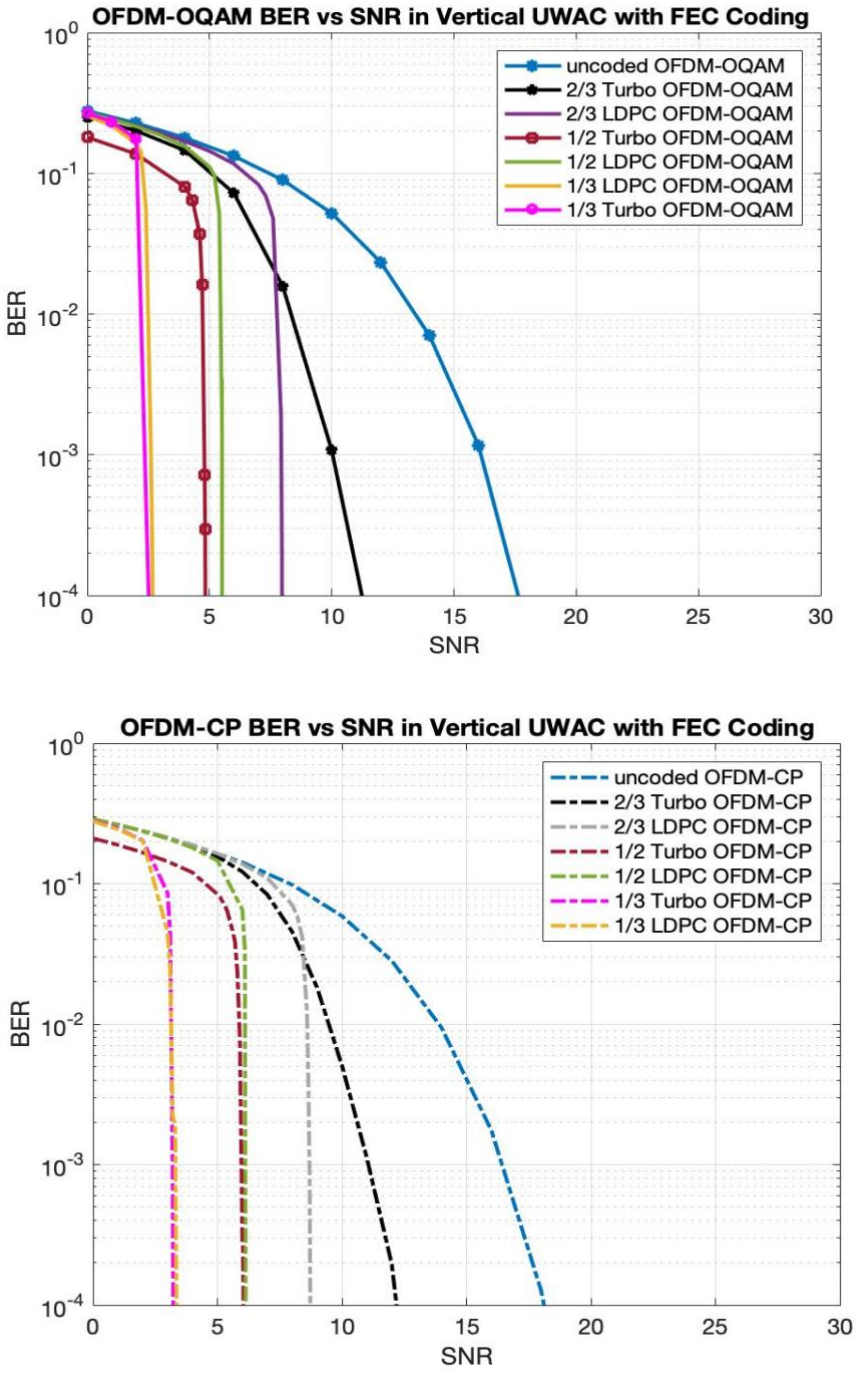


Figure 27- Extracted Results From Figure 26

Figures 27 shows the BER performance of each system extracted from figure 26 for clarity. In both cases low rate turbo codes (1/3 and ½) either outperform or have identical performance compared to LDPC codes of the same rate. Interestingly, as the code rate is increased LDPC codes begin to outperform turbo codes. For example, OFDM-OQAM system 2/3 LDPC outperforms OFDM-OQAM 2/3 turbo by 2.1dB at a BER of $10^{-3}$.

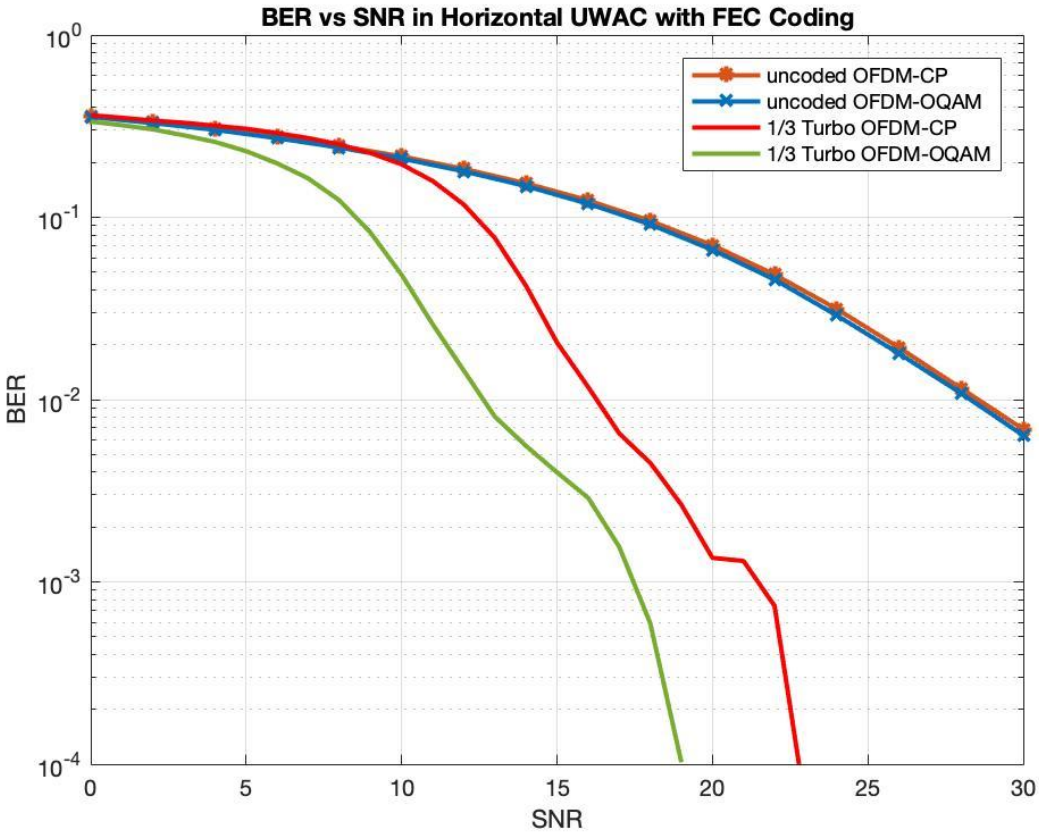


Figure 28-BER vs SNR (dB) in Horizontal UWAC with FEC

Figure 28 shows the BER performance of each system with 1/3 rate turbo codes used in the horizontal UWAC. It proved difficult to attain realistic results for ½ and 2/3 rate turbo codes along with LDPC codes due to the computational requirements of each simulation. Nonetheless figure 28 shows that coded OFDM-OQAM outperforms coded OFDM-CP by 4dB at a BER of $10^{-3}$. It can also be seen that the BER performance of 1/3 rate turbo codes is worse in this channel compared to the vertical channel simulated in figure 26. This is expected as the horizontal channel is more dispersive than the vertical channel and thus there are more bit errors for the same SNR. The poor BER performance of figure 28, even with low

rate powerful codes used, proves that other methods should be investigated to improve performance such as multiple input multiple output (MIMO) techniques.

## 5.2 THROUGHPUT PERFORMANCE

Having evaluated the BER performance of each system in horizontal and vertical UWACs the throughput performance of each system was investigated.

System throughput is calculated using the following equation:

$$D_{Th} = R \cdot \frac{N}{T_b + T_g} \cdot k$$

Equation 26

where R is the code rate, N is the number of subcarriers, $T_b + T_g$ is the symbol period and k is the number of bits per symbol. $k = \log_2 M$ , where M is the constellation size e.g. M=64 for 64 QAM. NB: $T_g = 0$ for OFDM-OQAM. In each OFDM-CP system, $T_g = 10$ms. The bandwidth = 115KHz.

| System Type | Number of Subcarriers N | Subcarrier Spacing $\Delta f$(Hz) | $T_g$ (ms) | $T_b$ (ms) | Spectral Efficiency (%) |
|---|---|---|---|---|---|
| **OFDM-CP** | 8192 | 14.03 | 10 | 71.2 | 87.7 |
| | 16384 | 7.01 | 10 | 142 | 93.4 |
| **OFDM-OQAM** | 8192 | 14.03 | N/A | 71.2 | 100 |
| | 1634 | 7.01 | N/A | 142 | 100 |

Table 5- Spectral Efficiency Performance

| Number of Subcarriers N | System Type | Modulation Type | Code Rate R | | | |
|---|---|---|---|---|---|---|
| | | | Uncoded | 1/3 | 1/2 | 2/3 |
| 8192 | OFDM-CP | QPSK | 196.92 | 65.64 | 98.46 | 131.28 |
| | | 16QAM | 393.85 | 131.28 | 196.92 | 262.56 |
| | | 64QAM | 590.77 | 196.92 | 295.38 | 393.85 |
| | OFDM-OQAM | QPSK | 230.11 | 76.70 | 115.10 | 153.41 |
| | | 16QAM | 460.22 | 153.41 | 230.11 | 306.82 |
| | | 64QAM | 690.34 | 230.11 | 345.17 | 460.22 |
| 16384 | OFDM-CP | QPSK | 212.78 | 70.93 | 106.39 | 141.85 |
| | | 16QAM | 425.56 | 141.85 | 212.78 | 283.71 |
| | | 64QAM | 638.34 | 212.78 | 319.17 | 425.56 |
| | OFDM-OQAM | QPSK | 230.76 | 76.92 | 115.38 | 153.84 |
| | | 16QAM | 461.52 | 153.84 | 230.76 | 307.68 |
| | | 64QAM | 692.28 | 230.76 | 346.14 | 461.52 |

Table 6- Throughput Performance of OFDM-CP vs OFDM-OQAM in KBits/S

Table 6 shows each system's throughput under a variety of coding rates and modulation schemes. Firstly it can be seen that OFDM-OQAM achieves a much greater throughput compared to OFDM-CP. This was as expected and is because OFDM-OQAM is able to effectively limit ISI and ICI without the need for a cyclic prefix. This enables more data to be transmitted per second, since the symbol period for OFDM-OQAM is smaller compared to that of OFDM-CP, for the same number of subcarriers and bandwidth. This is particularly attractive in UWACs which have a large delay spread in which the cyclic prefix is very long.

Secondly, both OFDM-CP and OFDM-OQAM systems with 16384 subcarriers exhibited higher throughput than their equivalent systems with 8192 subcarriers. Despite this, it is important to note that, as the number of subcarriers is increased, the frequency spacing $\Delta f$ between adjacent subcarriers is reduced. This increases system sensitivity to Doppler shifts and frequency synchronisation issues which could result in catastrophic ICI.

It can further be seen that throughput decreases with lower code rates. This is because lower rate codes have higher redundancy with less useful data transmitted. In erroneous channels,

such as the shallow horizontal underwater channel depicted in figure 23, lower rate codes should be used to effectively limit bit errors. Alternatively, higher rate codes should be used in less erroneous channels such as the vertical UWAC in order to maximise throughput while still limiting bit errors.
It is important to note that the QOS required at the receiver has an impact on which coding rate and system parameters should be used. For applications such as video transmission the lowest BER rate should be sought because single bit errors can cause entire video packets to be corrupted. This can be achieved by using lower rate codes however this limits the throughput. Overall, communications engineers must find the middle ground, such that sufficient throughput is achieved and bit errors are effectively reduced.

## 5.3 ZERO FORCING EQUALISATION ANALYSIS

In all previous simulations ZF equalisation was used with perfect channel knowledge. In reality, perfect channel knowledge is rarely the case. Figure 29 shows the BER performance of OFDM-CP in a 5 tap Rayleigh fading channel with a variety of pilot spacings. 2048 subcarriers were used with 16QAM modulation. Pilots were arranged in the comb type formation.

It is clear that as the number of pilot subcarriers is reduced (with larger pilot spacing) BER performance drastically reduces. This is because with larger pilot spacing the accuracy of the interpolation operation, conducted to find all subcarrier channel estimates, decreases. This causes channel estimates to be less accurate thus resulting in more errors after equalisation. In addition to this, it is important to note that pilot subcarriers reduce the achievable throughput as they transmit redundant data. For example, with a pilot spacing equal to 4 the throughput is reduced by exactly a quarter, since every $4^{th}$ subcarrier is a pilot. In the simulation shown below, the best system to use would be the system with pilot spacing equal to 64. This is because it exhibits very similar BER performance to the pilot spacing equal to 4, but achieves 16 times the throughput.

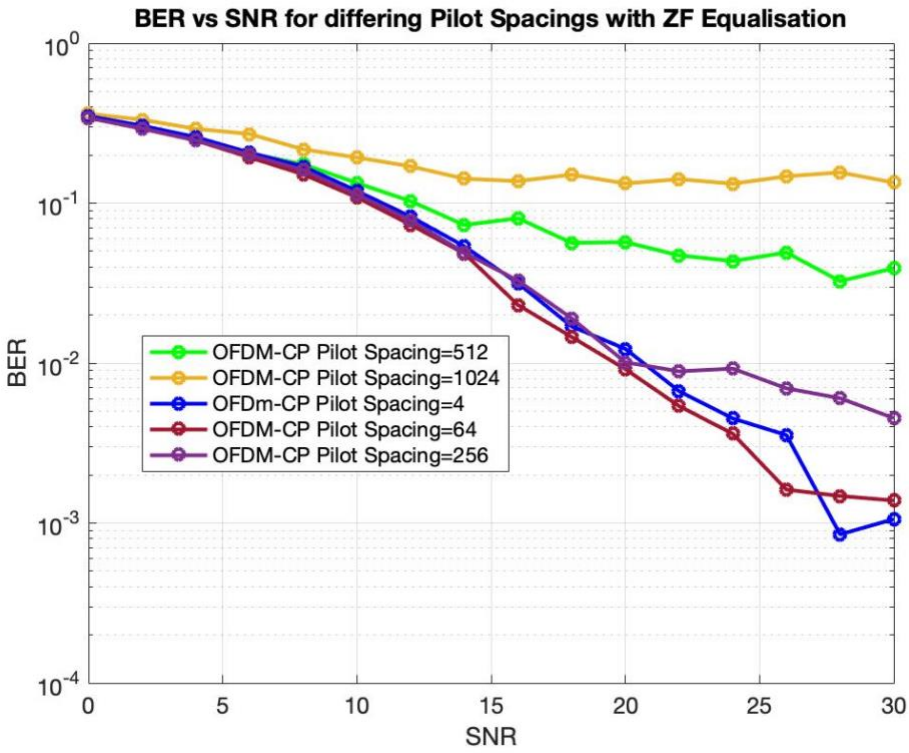


Figure 29- BER vs SNR (dB) for Differing Pilot Spacings

# CONCLUSIONS & FUTURE WORK

## 6.1 CONCLUSIONS

This research was designed to investigate the performance of OFDM-CP and OFDM-OQAM systems in the UWAC. Communications in the UWAC have been shown to be particularly challenging with the attenuation of acoustic waves being both frequency and distance dependent. This leads to difficulties in achieving high throughput since the UWAC has a very limited available bandwidth. Additionally, acoustic waves in the UWAC suffer significant time dispersion as a result of multipath propagation which, if uncorrected, can cause ISI.

With the above factors in mind, a communication system that is robust against ISI while also offering high spectral efficiency is required. OFDM-CP was selected as one type of system to be used due to its high spectral efficiency and robustness against ISI.

A second system, namely OFDM-OQAM, was also chosen to be designed, built and simulated. OFDM-OQAM is an alternative to OFDM-CP with the addition of filter banks at the transmitter and receiver. Provided these filter banks are well localised in time and frequency it is possible to limit ISI without the need of a cyclic prefix.

Each system was simulated in two different types of channel; the shallow horizontal UWAC and the vertical UWAC. The former had a depth of 25m and a transmission distance of 100m between transmitter and receiver while the latter had a depth of 200m and a transmission distance of 193m. The horizontal channel applied a delay spread to the signal as well as attenuation while the vertical channel assumed single path transmission because multipath propagation is more relaxed in this channel. The absorption coefficient and speed of sound in water were calculated using the Fisher and Simmons model and Mackenzie's equation respectively.

This research revealed that for the same number of subcarriers, bandwidth and modulation scheme OFDM-OQAM exhibited better throughput performance. For example, uncoded 16QAM OFDM-OQAM with 8192 subcarriers had a theoretical bit rate of 460.22Kbits/s while the equivalent OFDM-CP system had a bit rate of 393.85Kbits/s. This is an

improvement of 16.85% which is very appealing in the UWAC where it is difficult to achieve high throughput.

The BER performance of OFDM-CP and OFDM-OQAM was identical for QPSK, 16QAM and 64QAM modulation schemes in horizontal and vertically configured channels. This showed that OFDM-OQAM could effectively reduce ISI without the need for a cyclic prefix. Moreover, it confirms that the PHYDAS prototype filter used can prevent ICI in the frequency selective horizontal channel. A further simulation was conducted in a Rayleigh fading channel to test the ability of the cyclic prefix to remove ISI. When the cyclic prefix length was shorter than the number of channel taps BER performance significantly degraded. This highlighted the importance and therefore requirement to have a cyclic prefix in OFDM-CP systems to remove ISI.

With powerful FEC codes such as turbo and LDPC applied significant coding gains were made at the cost of lower achievable throughput. It was shown that in more dispersive channels, such as the horizontal channel, lower rate codes should be used in order to improve BER performance. In less dispersive channels, where there are less errors, higher rate codes such as 2/3 turbo/ LDPC should be used to improve the achievable throughput. It was also noted that coded OFDM-OQAM outperformed coded OFDM-CP for equivalent coding type and rates.

1/3 and ½ rate turbo codes were shown to perform very similarly if not slightly better than LDPC codes of the same rate in both systems tested. However, as the coding rate was increased to 2/3, LDPC codes outperformed turbo codes by up to 3.5dB at a BER of $10^{-4}$. Therefore, as a result of this, large block length LDPC codes should be the preferred choice when higher rate codes are required. Alternatively, where lower rate codes are required in more dispersive channels, then turbo codes should be used.

In terms of equalisation OFDM-CP is less complex than OFDM-OQAM. OFDM-CP can be seen to convert a wideband channel into many equally spaced narrowband channels. If the number of subcarriers is sufficiently high, flat fading occurs. This allows for simple zero forcing equalisation. In contrast, OFDM-OQAM requires more complex equalisation to prevent ISI between the adjacently transmitted real and imaginary parts.

The BER performance of OFDM-CP with different equalisation parameters was simulated. It showed that ZF equalisation with perfect channel knowledge outperformed equalisation without perfect channel knowledge. Perfect channel knowledge is not realistic, and as such pilots must be used to attain channel knowledge. BER performance was much better with smaller pilot subcarrier spacing however this results in more subcarriers being used for redundant data and thus a reduction in achievable throughput. A trade off must be made between achieving accurate channel knowledge while ensuring throughput is sufficient.

Overall OFDM-OQAM is an attractive alternative to OFDM-CP for underwater acoustic communications. It provides higher throughput than equivalent OFDM-CP systems while exhibiting similar, if not improved, BER performance. Furthermore, OFDM-OQAM is less sensitive to Doppler shifts which are typically very large in the UWAC due to the low propagation speed of acoustic waves. In spite of this, OFDM-OQAM is more complex with the addition of filter banks and requires very much more complex equalisation methods.

## 6.2 FUTURE WORK

One area of future work is to improve the accuracy of the channels used in simulations. For example, all simulations assumed the UWAC to have negligible Doppler effect in addition to perfect timing and frequency synchronisation between transmitter and receiver. In reality this would not be the case, since the Doppler effect in the UWAC is typically very large. Indeed, it is known that even a very small change in the relative velocity between transmitter and receiver in the UWAC can increase the BER. In future work the Doppler effect of the UWAC should be introduced with Doppler estimation and compensation algorithms also implemented. To this day active research is being carried out to reduce system sensitivity to Doppler in the UWAC. This includes block-Doppler and multiple re-sampling compensation techniques [33] [34].

Additionally, for simplification, AWGN was used as a substitute for ambient noise in each channel. In future work, a more accurate mathematical model of ambient noise should be implemented to improve the accuracy of channel simulations.

In this thesis simple zero forcing equalisation was used to reduce ISI however this technique is prone to noise amplification in frequency selective channels. In future work more accurate

equalisation techniques should be used for UWA communications such as MMSE and decision feedback equalisation (DFE). MMSE shares many similarities with ZF but effectively measures the SNR of the signal such that, in deep fades, noise amplification is prevented. In addition to this, DFE using least mean squares (LMS) has proven to exhibit very good performance in a variety of UWACs especially with a coherent receiver [35] [36]. Recently, blind equalisation methods have been an area of consistent research. Blind equalisation does not require pilot carriers to be used for channel estimation, so more subcarriers can be actively used for data transmission. This is very attractive in band limited channels such as the UWAC but is complex and suffers from slow convergence [37].

The BER and throughput performance of each system can be significantly improved with the introduction of multiple input multiple output (MIMO). MIMO has proven revolutionary in the communications industry and adopts multiple antennae at both the transmitter and receiver. In the case of underwater communications, much improved throughput and BER performance is achieved by using multiple hydrophones. Moreover it has been shown that MIMO-OFDM-OQAM outperforms MIMO-OFDM-CP by up to 4dB at a BER of $10^{-3}$. Despite this MIMO-OFDM-OQAM represents a challenge for channel estimation [38].

Filtered Multi Tone (FMT) has been considered for underwater communications. In a similar way to OFDM-CP and OFDM-OQAM, FMT splits the available bandwidth into many sub bands however these bands do not overlap. Almost perfect spectral containment is achieved with the addition of pulse shaping filters well localised in frequency and time. In addition to this, FMT tends to use a smaller number of subcarriers, so subcarrier spacing is much higher. This results in FMT being very robust against ICI and less sensitive to Doppler and frequency synchronisation problems at the cost of spectral efficiency [38].

# REFERENCES


[1] S. Zhou and Z. Wang, OFDM for underwater communications, Chichester, West sussex: Wiley, 2014.

[2] W.J.Broad, “Nytimes.com,” 3 September 1985. [Online]. Available: www.nytimes.com/1985/09/03/science/wreckage-of-titanic-reported-discovered-12000-feet-down.html.

[3] C. Xu, Z. Zheng and C. Ji, “Practical Deployments of SEMAT on Wireless Sensor Networks in the marine Environment,” in *2013 IEE 9th international Conference on Mobile Ad-hoc and Sensor Networks*, 2013.

[4] J. Trubuil and T. Chonavel, “Accurate Doppler estimation for underwater acosutic communications,” in *2012 Oceans* , Yeosu, 2012.

[5] M. Stojanovic and J. Preisig, “Underwater acustic communication channels: Propagation models and statistical characterization,” *IEEE Communications magazine,* vol. 47, no. 2, pp. 84-89, 2009.

[6] m. Anjum, “Underwater acoustic channel modelling, simulation and estimation,” in *International Bhurban Conference on Applied Sciences and Technology*, 2011.

[7] A. Sehgal, I. Tumar and J. Schonwalder, “Aquatools: An underwater acustic networking simulation toolkit,” in *IEEE Oceans*, Sydney, 2012.

[8] m. Domingo, “overview of channel models for underwater wireless networks,” *Elsevier Journal on physical communication,* vol. 1, no. 3, pp. 163-182, 2008.

[9] L. Vall and M. Stojanovic, “Short paper: Towards underwater video transmission.,” Cambridge, MA; Sea Grant College program, Massachusetts institute of Technology, 2011.

[10] M. Chitre, J. Potter and S. Ong, “Optimal and Near-optimal Signal Detection in Snapping Shrimp Dominated Ambient Noise,” *IEE Journal of Oceanic Engineering,* vol. 31, no. 2, pp. 497-503, 2006.

[11] X. Zhang, X. Han, J. Yin and X. Sheng, “Study on Doppler effects estimate in underwater acosutic communication,” 2013.

[12] J. Ribas, “Underwater Wireless Video Transmission using acoustic OFDM,” *Master of Science Thesis , Massachusetts Institute of Technology,* 2010.

[13] N. Lasorte, W. Barnes and H. Refai, “The History of Orthogonal Frequency Division Multiplexing,” in *IEE Global Telecommunications Conference 2008*, 2008.

[14] S. Weinstein, “The history of orthogonal frequency division multiplexing,” *IEE Communications Magazine ,* vol. 47, no. 11, pp. 26-35, 2009.

[15] A. Agarwal and S. Patra, “Performance prediction of OFDM based DAB system using block coding techniques,” in *2011 International Conference on Emerging Trends in Electical and Computer Technology* , 2011.

[16] J. Remy and C. Letamendia, “LTE Standards,” London, 2014.

[17] E. T. S. I. (ETSI), “Digital Video broadcasting: second generation framing structure, channel coding and modulation systems for broadcasting, interactive services, news gathering and other broadband satellite applications”.

[18] B. Muquet, Z. Wang, G. Giannikis, M. Courville and P. Duhamel, “Cyclic Prefixing or zero padding for wireless multicarrier transmissiom?,” *IEE Transactions on Communications,* vol. 50, no. 12, pp. 2136-2148, 2002.

[19] S. S. Division, “Digital Video Broadcasting (DVB); framing structure, channel coding and modulation for digital terrestrial television,” Pretoria, 2011.

[20] R. Van Nee and R. Prasad, OFDM for wireless multimedia communications, Boston: Artech House, 2000.

[21] S. Chen, G. Dai and T. Yao, “Zero-forcing equalisation for OFDM systems over doubly-selective fading channels using frequency domain redundancy,” *IEE Transactions on Consumer Electronics``,* vol. 50, no. 4, pp. 1004-1008, 2004.

[22] C. P. Berrou, P. Adde, C. Douillard and R. Bidan, “ECWT: An Overview of Turbo Codes and there applications,” in *The European Conference on Wireless technology*, 2005.

[23] R. Baby, “Convolution coding and applications: A performance analysis under AWGN channel,” in *International Conference on Communication networks (ICCN)*, 2015.

[24] Pietrobon, “On punctured serially cocatenated turbo codes,” in *35th Asilomar Conference on Signals, systems and computers*, 2001.

[25] G. Oletu and P. Rapaiic, “The performance of turbo codes for wireless communication systems,” in *3rd international Conference on Computer Research and Development*, 2011.

[26] Z. Tu and S. Zhang, “overview of LDPC codes,” in *7th IEEE international Conference on Computer and Information technology*, 2007.

[27] K. Andrews, “The development of turbo and LDPC codes for deep space applications,” *Proceedings of IEEE,* vol. 95, no. 11, pp. 2142-2156, 2007.

[28] B. Saltzberg, “Performance of an Efficient Parallel Data Transmission System,” *IEEE Transactions on Communication technology ,* vol. 15, no. 6, pp. 805-811, 1967.

[29] M. a. p. Bellanger, “FBMC physical layer; ap primer,” 2010.

[30] Bale.R, R. Y. Seetharamaiah, A. Dubey and T. Panigrahi, “OFDm vs FBMC: A comparative analysis for broadband-PLC,” in *2018 10th International Conference on Communication Systems & Networks*, 2018.

[31] M. Bocus, A. Doufexi and D. Agrafiotis, “Performance evaluation of filterbank multicarrier systems in an underwater acoustic channel,” in *27TH Annual International Symposium on personal, Indoor and Mobile Radio Communications*, 2016.

[32] M. Aldababseh and A. Jamoos, “Estimation of FBMC/OQAM fading channels using dual Kalman filters,” *The Scientific World Journal,* 2014.

[33] A. Abdelkareem, B. Sharif, C. Tsimenidis, J. Neasham and O. Hinton, “Doppler compensation for OFDM-based underwater acoustic communication systems,” in *Oceans 2011 IEEE*, Spain 2011, 2011.

[34] B. Karakaya, M. Hasna, T. Duman, M. Uysal and Ghrayeb, “Multi resampling Doppler Compensation in cooperative underwater OFDM systems,” in *MTS/IEEE OCEANS*, Bergen 2013, 2013.

[35] L. Zhong and N. Xiao-Ling, “Comparison of equalization algorithms for underwater acoustic channels,” in *2nd international Conference on Computer Science and Network technology*, 2012.

[36] M. Stojanovic, J. Catipovic and J. Proakis, “Adaptive multichannel combining and equalisation for underwater acoustic communications,” *The Journal of the acoustical society of america ,* vol. 94, no. 2, pp. 1621-1631, 1993.

[37] V. Savaux and F. Bader, “Sub-optimal initialization for blind equalization with fast convergence in OFDM-OQAM modulation,” in *2015 European Conference on Networks and Communications*, 2015.

[38] M. J. Bocus, D. Agrafiotis and A. Doufexi, “Underwater acoustic video transmission using MIMO-FBMC,” in *2018 OCEANS- MTS/IEEE Kobe Techno-Oceans*, 2018.

# APPENDIX I

## SOFTWARE DECLARATION

| Filename/Algorithm/ Package | Supplier/Source/Author/ website | Use/Modifications made/ Student written |
|---|---|---|
| Hor_chan | J Bocus | Used for channel simulations. No modifications |
| Ver_chan | J Bocus | Used for channel simulations. No modifications |
| *OFDM-CP-AWGN* | J Perrin | Student Written |
| *OFDM-CP-RAY* | J Perrin | Student Written |
| *OFDM-CP-UWA* | J Perrin | Student Written |
| *OFDM-ZF* | J Perrin | Student Written |
| OFDM-OQAM-UWA | All OFDM-OQAM scripts were modified from J Bocus previous work. | Modifications made included alternative filter design and use of FEC coding. |
| OFdm-OQAM-AWGN | | |
| OFDM-OQAM-RAY | | |

The README.txt file contained on this memory stick contains more details of MATLAB files used and there respective owner.